Reward contingency gates selective cholinergic suppression of amygdala neurons

Eyal Y. Kimchi[1,2]*, Anthony Burgos-Robles[1,3], Gillian A. Matthews[1], Tatenda Chakoma[1], Makenzie Patarino[1], Javier Weddington[1], Cody A. Siciliano[1,4], Wannan Yang[1], Shaun Foutch[1], Renee Simons[1], Ming-fai Fong[5], Miao Jing[1,6], Yulong Li[7], Daniel B. Polley[8,9], Kay M. Tye[1,10,11,12,13]*

[1] The Picower Institute for Learning and Memory, Department of Brain and Cognitive Sciences, Massachusetts Institute of Technology, Cambridge, MA 02139, USA

[2] Department of Neurology, Northwestern University, Chicago, IL 60611, USA

[3] The Department of Neuroscience, Developmental, and Regenerative Biology, Neuroscience Institute & Brain Health Consortium, University of Texas at San Antonio, San Antonio, TX 78249, USA

[4] Vanderbilt Center for Addiction Research, Department of Pharmacology, Vanderbilt University, Nashville, TN 37232 USA

[5] Coulter Department of Biomedical Engineering, Georgia Tech & Emory University, Atlanta, GA 30332 USA

[6] Chinese Institute for Brain Research, Beijing 102206, China

[7] State Key Laboratory of Membrane Biology, Peking University School of Life Sciences; PKU-IDG/McGovern Institute for Brain Research; Peking-Tsinghua Center for Life Sciences, Beijing 100871, China

[8] Eaton-Peabody Laboratories, Massachusetts Eye and Ear Infirmary, Boston, MA 02114, USA

[9] Department of Otolaryngology – Head and Neck Surgery, Harvard Medical School, Boston, MA 02114, USA

[10] The Salk Institute for Biological Studies, La Jolla, CA 92037, USA

[11] Howard Hughes Medical Institute, The Salk Institute, La Jolla, CA 92037, USA

[12] Kavli Institute for Brain and Mind, La Jolla, CA 92037, USA

[13] Lead Contact

*Correspondence: eyal.kimchi@northwestern.edu, @ekimchi (E.Y.K.) and tye@salk.edu, @kaymtye (K.M.T.)

Abstract

Basal forebrain cholinergic neurons modulate how organisms process and respond to environmental stimuli through impacts on arousal, attention, and memory. It is unknown, however, whether basal forebrain cholinergic neurons are directly involved in conditioned behavior, independent of secondary roles in the processing of external stimuli. Using fluorescent imaging, we found that cholinergic neurons are active during behavioral responding for a reward – even in prior to reward delivery and in the absence of discrete stimuli. Photostimulation of basal forebrain cholinergic neurons, or their terminals in the basolateral amygdala (BLA), selectively promoted conditioned responding (licking), but not unconditioned behavior nor innate motor outputs. *In vivo* electrophysiological recordings during cholinergic photostimulation revealed reward-contingency-dependent suppression of BLA neural activity, but not prefrontal cortex (PFC). Finally, ex vivo experiments demonstrated that photostimulation of cholinergic terminals suppressed BLA projection neuron activity via monosynaptic muscarinic-receptor-signaling, while also facilitating firing in GABAergic interneurons. Taken together, we show that the neural and behavioral effects of basal forebrain cholinergic activation are modulated by reward contingency in a target-specific manner.

Keywords

Acetylcholine, Basal Forebrain, Basolateral amygdala, Prefrontal cortex, Limbic networks, Motivated behavior, Conditioning, Reward

Introduction

Acetylcholine (ACh) is a powerful neuromodulator thought to influence how the brain processes and learns about external stimuli (Ballinger et al., 2016; Higley and Picciotto, 2014; Likhtik and Johansen, 2019; Newman et al., 2012). The basal forebrain is a prominent source of cholinergic innervation of the entire cortical mantle, as well as related telencephalic structures such as the amygdala (Gielow and Zaborszky, 2017; Li et al., 2018). Most work on basal forebrain cholinergic circuits to date has focused on how ACh modifies the processing of other stimuli, either by increasing attention to conditioned stimuli (Bakin and Weinberger, 1996; Baxter and Chiba, 1999; Gritton et al., 2016; Pinto et al., 2013), or by enhancing associations between conditioned stimuli and unconditioned stimuli/reinforcers in learning and memory (Ballinger et al., 2016; Crouse et al., 2020; Guo et al., 2019; Jiang et al., 2016; Letzkus et al., 2011; Sturgill et al., 2020). In contrast, less work has been done to explore the behavioral effects of basal forebrain cholinergic neuron activation in the absence of external stimuli (Aitta-Aho et al., 2018). As a result, in most models of cholinergic function, the behavioral relevance of basal forebrain cholinergic neuron activity in the absence of discrete external stimuli is comparatively less specified (Hasselmo and Sarter, 2011; Thiele and Bellgrove, 2018).

Basal forebrain cholinergic projections have considerable physiological effects on post-synaptic neurons *ex vivo,* where sensory stimuli cannot be presented (Kalmbach et al., 2012; Venkatesan et al., 2020). Basal forebrain cholinergic projections have prominent direct effects on limbic circuits (Venkatesan et al., 2020), including the basolateral amygdala (BLA) (McDonald and Mascagni, 2011, 2010; Unal et al., 2015). *Ex vivo* optogenetic activation of the cholinergic projection to the BLA affects post-synaptic activity differentially, suppressing neural activity at low firing rates (Unal et al., 2015). In contrast, however, *in vivo* cholinergic activation may increase spontaneous BLA neural firing (Jiang et al., 2016), suggesting that the post-synaptic effects of basal forebrain cholinergic projections may be depend upon as yet unidentified influences. We therefore sought to understand how basal forebrain cholinergic neuron activation, in the absence of discrete, environmental stimuli, may affect both behavior and downstream neural activity. To do this, we developed a new behavioral paradigm allowing us to study the short-time scale effects of basal forebrain cholinergic neurons on behavior in the absence of other discrete external cues. We sought to identify features that may regulate the effects of acetylcholine on behavior and downstream neural circuit activity.

Results

Establishing conditioned behavior in the absence of discrete cues

To study whether basal forebrain cholinergic neurons affect conditioned behavior in the absence of discrete cues, we developed a new behavioral paradigm, which we refer to as the Windows of Opportunity Task (WoOT) (Figure 1A). During WoOT, mice were head-fixed mice in front of a spout, with a goal of establishing a steady level of behavioral engagement, as measured by licking. WoOT sessions were divided into “trials” of 3-second *Windows of Opportunity*, with intervening variable intertrial intervals (ITIs). Rewards were only delivered if mice licked the spout during an unsignaled *Window of Opportunity*. Because rewards were only delivered *after* the first lick in a *Window of Opportunity*, and because windows were not discretely cued and occurred with variable ITIs, mice did not know whether any given lick would be rewarded. The underlying task structure of this task is an operant, variable-interval reinforcement schedule with limited hold (Ferster and Skinner, 1957). In this operant schedule, unsignaled reward opportunities become available after a variable interval (ITI), but only for a limited time (“hold” in original terminology, “window” in our terminology here).

Training mice in this manner conditioned them to lick the spout with a relatively stable pattern of intermittent lick bouts (Figure 1B), which we designate as “conditioned responding,” using the formal operant sense (Ferster and Skinner, 1957). In addition to the *Windows of Opportunity*, we also defined a series of *Unrewarded Windows*, on which, even if the mouse licked, reward would not be delivered—equivalent to the intervening ITI (Figure 1A-B). While these *Unrewarded Windows* practically functioned as part of the ITI, they were programmatically necessary to study behavior in a way that matched the temporal characteristics of the *Windows of Opportunity*, but when reward was not available.

Prior to initial training, mice underwent surgery to prepare them for head-fixation and subsequent photostimulation of basal forebrain cholinergic neurons, using Cre-dependent expression of either optogenetic Channelrhodopsin-2 (ChR2) or a control fluorophore (enhanced yellow fluorescent protein, eYFP) (Figure 1C-D). Fibers were implanted to target the sublenticular substantia innominata/extended amygdala, the posterior portion of the basal forebrain whose cholinergic neurons project to the BLA and cortical mantle (Rye et al., 1984; Zaborszky et al., 2012). Nearly 90% of neurons expressing ChR2 were cholinergic, as confirmed by immunostaining for choline acetyltransferase (ChAT), an obligate enzyme in the synthesis of ACh (Prado et al., 2002) (Figure S1A-B). During early WoOT training, which did not yet involve photostimulation, mice were trained for a mean of 7 sessions (Figure S1C), and both ChR2 and eYFP mice were similarly likely to lick at least once on an unsignaled *Window of Opportunity* as on an *Unrewarded Window*, confirming that mice could not predict reward delivery prior to licking, and that viral expression in the absence of photostimulation did not influence behavior (Figure S1D). Prior to photostimulation, ChR2 and eYFP groups also collected similar numbers of rewards (Figure S1E), had similar lick rates over entire sessions (Figure S1F), and had similar lick bout characteristics (Figure S1G-I), suggesting a stable setting in which to study the effects of transient photostimulation of cholinergic basal forebrain neurons.

Transient photostimulation of basal forebrain cholinergic neurons increases conditioned responding when paired with the opportunity to collect rewards

After mice had undergone initial WoOT training, we were then able then investigate whether transient photostimulation of basal forebrain cholinergic neurons affected conditioned responding under different conditions (Figure 1E-G). We first tested whether photostimulation of basal forebrain cholinergic neurons inherently affected licking by delivering 2 sec of photostimulation exclusively during *Unrewarded Windows*, i.e., when licking would not be reinforced (Photostim-Unreinforced session, Figure 1F). In these Photostim-Unreinforced sessions, licking did not increase during photostimulated windows compared to windows with no photostimulation, in either ChR2 or eYFP mice (Figure 1H).

In separate sessions, we tested whether transient photostimulation of basal forebrain cholinergic neurons affected licking when photostimulation was delivered exclusively during a subset of unsignaled *Windows of Opportunity*, i.e., when licking would be reinforced (Figure 1G, Photostim-Reinforced session, right panel). Given that there was no discrete external cue for these windows, we had initially hypothesized that cholinergic basal forebrain photostimulation would not impact licking behavior. However, in these Photostim-Reinforced sessions, photostimulation increased licking in mice expressing ChR2, but not eYFP (Figure 1I). In contrast, during windows with no photostimulation, licking remained similar between ChR2 and eYFP mice (Figure 1I). Transient photostimulation of basal forebrain cholinergic neurons became capable of promoting an operant conditioned response, increasing the likelihood and decreasing the latency of licking, but only after being paired with the opportunity to collect rewards.

While we initially used photostimulation parameters similar to prior work (Herman et al., 2016; Jiang et al., 2016), we also examined whether even briefer photostimulation of cholinergic basal forebrain neurons was sufficient to affect conditioned responding. In a separate session, we randomly delivered photostimulation on *Windows of Opportunity* using either 0, 1, 2, or 10 pulses at 20 Hz, corresponding to 5-500 ms of photostimulation (Figure 1J-K). Even a single 5 ms laser pulse was sufficient both to increase the likelihood of licking (Figure 1J) and to accelerate the latency of the first lick following photostimulation onset (Figure 1K). In summary, brief photostimulation of cholinergic basal forebrain neurons can promote conditioned responding when paired with potential reinforcement. Further examples and analyses of the licking behavior across the Photostim-Unrewarded and Photostim-Rewarded sessions are depicted in Figure S2 and Figure S3.

Photostimulation of basal forebrain cholinergic neurons does not increase unconditioned movement and is not inherently reinforcing

Given that photostimulation of basal forebrain cholinergic neurons drove conditioned behavior when paired with potential reinforcement, we performed a series of experiments to determine whether the effects of photostimulation were specific to conditioned responding. We first examined whether photostimulation of cholinergic neurons increased other types of movement, for example locomotion in an unreinforced context. Basal forebrain cholinergic photostimulation did not increase locomotion in an open field test (OFT, Figure S4A-B), as measured by mouse velocity (Figure S4C). Additionally, photostimulation did not modify innate location preference, as measured by the amount of time spent in the center of the open field, which was avoided similarly by ChR2 and eYFP mice (Figure S4D).

We next assessed whether photostimulation of cholinergic basal forebrain neurons inherently reinforced other types of locomotor behavior (Figure S4E). Mice were freely allowed to explore a chamber in which one half was paired with photostimulation, in a Real-Time Place Preference assay (RTPP). Neither ChR2 nor eYFP mice demonstrated a preference for the side paired with photostimulation, suggesting that photostimulation of cholinergic basal forebrain neurons was not inherently reinforcing (Figure S4F).

Since cholinergic photostimulation did not increase movement in unreinforced contexts, we also tested whether cholinergic photostimulation affected unconditioned movements within our reinforced, behavioral task context. A subset of mice was trained while on a treadmill, in order to measure spontaneous, unconditioned locomotion. There was no difference in locomotion around the time of photostimulation between ChR2 and eYFP mice, during either Photostim-Unreinforced or Photostim-Reinforced sessions (Figure S4G). Locomotion also did not differ significantly between Photostim-Unreinforced and Photostim-Reinforced sessions, for either ChR2 or eYFP mice (Figure S4H).

Lastly, we examined whether photostimulation of cholinergic basal forebrain neurons increased arousal during our head-fixed task, as measured by pupil diameter, using machine learning based pupillometry (DeepLabCut, Figure S4I-L). During Photostim-Unreinforced sessions, photostimulation of cholinergic neurons caused a modest increase in pupil dilation in ChR2 mice compared to eYFP mice (Figure S4I, left; rank-sum between groups, $p<0.05$). The first significant difference in pupil size between ChR2 and eYFP mice began 1.2 sec after laser onset. During Photostim-Reinforced sessions, photostimulation also caused an increase in pupil dilation in ChR2 mice compared to eYFP mice, now beginning 0.7 sec after laser onset (Figure S4I, right; rank-sum between groups, $p<0.05$). Pupil changes were larger during Photostim-Reinforced than Photostim-Unreinforced sessions for ChR2 mice (Figure S4J). There was no clear change in pupil size after photostimulation for eYFP mice (Figure S4J).

Some of the differences in photostimulation-evoked pupil dilation during the Photostim-Reinforced session for ChR2 mice may have been related to reward collection behavior. We examined pupillary diameter at the time of reward delivery in both Photostim-Unreinforced and Photostim-Reinforced sessions (Figure S4K). During both sessions, pupils dilated similarly in ChR2 and eYFP mice following reward delivery (Figure S4L). Therefore, cholinergic photostimulation increases arousal modestly, but this effect becomes evident more slowly for pupillary dilation than for licking behavior (0.5 sec latency for licking as in Figure 1).

Muscarinic receptors are necessary for conditioned responding

ACh can affect post-synaptic neurons in target regions through two classes of receptors: fast, ionotropic nicotinic receptors and relatively slower, G-protein coupled, metabotropic muscarinic receptors (Brown, 2019). In order to test which receptors mediated the effects of photostimulation of cholinergic basal forebrain neurons on conditioned responding, we blocked each receptor class using intraperitoneal injections of either a muscarinic antagonist (scopolamine) (Kruk et al., 2011; Kruk-Słomka et al., 2014) or a nicotinic antagonist (mecamylamine) (Adermark et al., 2014; Zachariou et al., 2001) (Figure 2A).

In order to understand the specific sensitivity of photostimulation induced licking, however, and to increase within-subject control, we used a different task structure, in which mice were also trained to respond to tones (i.e. where a tone indicated a *Window of Opportunity*) (Figure 2B)

prior to injections. On separate trials, mice received either a tone or transient photostimulation (2 sec duration each). If mice licked after the onset of the tone or after the onset of photostimulation (within 3 sec), they received a fluid reward. Licking after either tones or photostimulation was compared to licking on matched unrewarded windows during the ITI, a measure of baseline licking likelihoods. This more traditional operant task, using either tones or photostimulation, can be thought of as a variation of the WoOT operant task—in this version, there are no longer unsignaled windows: all windows are now potentially signaled by either Tones or Photostimulation, granting improved within subject control to assess the pharmacologic sensitivity of each trial type: tone, photostimulation, or baseline licking.

On a control day in which mice were injected with saline, both ChR2 and eYFP mice responded more during tones than during ITIs (Figure 2C). However, only optogenetic ChR2 mice responded more during Photostimulation than during ITIs, responding at similar rates during photostimulation as they did during tones.

When mice received an injection of the muscarinic receptor antagonist scopolamine (0.3mg/kg), however, ChR2 mice began to lick less during photostimulation than tones (Figure 2C, middle panels). With a higher dose of scopolamine (1mg/kg), ChR2 mice licked similarly on photostimulation trials as during ITIs, despite still licking more during tone trials than ITIs. Results from both doses suggested that blocking muscarinic receptors decreased conditioned responding (tones and photostimulation), but that conditioned responding to basal forebrain cholinergic neuron photostimulation was more sensitive to muscarinic blockade than conditioned responding to tones.

In contrast, conditioned responding to tones and photostimulation after injection of the nicotinic receptor antagonist mecamylamine was similar to that after saline control for both ChR2 and eYFP mice (Figure 2C, right). Therefore, muscarinic receptors, rather than nicotinic receptors, were necessary for conditioned responding to basal forebrain cholinergic neuron photostimulation.

Basal forebrain cholinergic neurons are active during conditioned responding

Having determined that photostimulation of basal forebrain cholinergic neurons can promote conditioned responding even in the absence of discrete external cues, we next examined whether basal forebrain cholinergic neurons are inherently active during conditioned responding. Basal forebrain cholinergic neurons have been described to be active during reinforcer delivery (Hangya et al., 2015), reward consumption (Harrison et al., 2016), movements including locomotion (Harrison et al., 2016; Nelson and Mooney, 2016), and conditioned stimuli (Guo et al., 2019; Parikh et al., 2007). However, we observed that photostimulation of basal forebrain cholinergic neurons increased conditioned responding independent of these factors: in the absence of conditioned cues, prior to reinforcer delivery or consumption, and without affecting unconditioned movements such as locomotion. We therefore studied whether basal forebrain cholinergic neuron activity also changes at the time of conditioned responding in the absence of reward, using a genetically-encoded fluorescent calcium indicator, GCaMP6s (Chen et al., 2013), as a proxy for neural activity.

We targeted expression of GCaMP6s to basal forebrain cholinergic neurons using virally-mediated, Cre-dependent expression (AAVdj-EF1a-DIO-GCaMP6s) (Figure 3A). An optic fiber implanted over the basal forebrain enabled real-time recording of fluctuations in neural activity

using fiber photometry (Adelsberger et al., 2005; Cui et al., 2013; Gunaydin et al., 2014; Lütcke et al., 2010). We recorded GCaMP6s fluorescence while mice performed a more traditional operant task to detect tones. Licking after the onset of tones (within 3 sec) was rewarded (Figure 3B). Recordings during this task demonstrated fluorescent transients in the 470 nm signal channel that appeared linked to behavioral events (Figure 3C). Peri-event analyses suggested that fluorescence levels increased at the time of behavioral events, most clearly with licking in the presence of a tone (Figure 3D-E), but also during spontaneous licking (i.e. in the absence of tone cues and reward delivery) (Figure 3F-G). There were no apparently meaningful changes in the 405 nm reference channel, suggesting that changes in fluorescence were not related to simple movement artifacts.

It is possible that basal forebrain cholinergic neuron activity during licking even in the absence of tone cues was in some way influenced by the broader cue-reinforcer association context of this task. To control for this, we also recorded fluorescent activity from basal forebrain cholinergic neurons prior to any experience with tone cues, during our uncued reward task (WoOT, Figure 3H). Even in this context, without discrete tones or cues, changes in fluorescent activity were observed both at the time of licking that triggered reward delivery (Figure 3I), as well as at the time of licking in the absence of reward delivery (Figure 3J-K). This suggests that cholinergic neurons are physiologically active at the time of conditioned responding, even in the absence of cues and reward consumption.

Local ACh levels in the BLA, measured using a genetically-encoded sensor, increase during conditioned responses

Although we had determined that basal forebrain cholinergic neuron activity increases with conditioned responding (Figure 3), we wanted to confirm whether ACh is released at these times into target regions. We measured ACh release within the BLA using a novel version of a genetically-encoded ACh sensor ($GRAB_{ACh3.0}$, abbreviated as GACh3.0 hereafter) (Jing et al., 2018), whose fluorescence reports the dynamics of extracellular ACh (Figure 4A-B), with somewhat faster kinetics than GCaMP6s (Chen et al., 2013).

We drove expression of the genetically-encoded ACh sensor in BLA neurons by injecting an adeno-associated virus carrying the ACh sensor (AAV_9-hSyn-GACh3.0) into the BLA (Figure 4A). An optic fiber implanted over the BLA enabled real-time recording of ACh dynamics in the BLA by fiber photometry. We recorded local ACh while mice performed a more traditional operant task to detect tones, during which licking after tone onset was rewarded (Figure 4C). Sample recordings during this task revealed fluorescent transients that appeared linked to behavioral events (Figure 4D). Similar to somatic GCaMP photometry, GACh3.0 fluorescence signals increased at the time of behavioral events, significantly for licking leading to reward delivery (Figure 4E-F). We also recorded BLA ACh dynamics prior to any experience with tone cues, during our uncued reward task (WoOT, Figure 4I). Even in this context, without discrete tones or other discrete cues, changes in fluorescent signals were observed both at the time of licking that triggered reward delivery, as well as at the time of licking without subsequent reward delivery (Figure 4J-L). These results suggest that BLA ACh levels increased at the time of conditioned responding, even in the absence of discrete cues and reward consumption.

Photostimulation of basal forebrain cholinergic terminals in the BLA increases conditioned behavior when paired with reinforcement

Having confirmed that ACh levels in the BLA increase at the time of conditioned responding, we next studied whether photostimulation of basal forebrain cholinergic terminals directly within the BLA was sufficient to promote conditioned responding. Using Cre-dependent targeting, we again expressed either ChR2 or a control fluorophore (eYFP) in basal forebrain cholinergic neurons (Figure 5A). To stimulate cholinergic terminals in the BLA, we placed an optic fiber over the BLA.

Following initial uncued training, we tested whether transient photostimulation of basal forebrain cholinergic terminals in the BLA affected conditioned responding under two different conditions. When photostimulation was performed during *Unrewarded Windows* (Photostim-Unreinforced sessions), licking did not increase compared to statistically matched baseline windows, in either ChR2 or eYFP mice (Figure 5B). When photostimulation was delivered exclusively during a subset of *Windows of Opportunity* (Photostim-Reinforced sessions), photostimulation increased licking only in mice expressing ChR2 (Figure 5C). Baseline licking rates, however, remained similar between ChR2 and eYFP mice. Hence, transient photostimulation of basal forebrain cholinergic terminals in the BLA drove conditioned responding in a temporally precise way, only when photostimulation was associated with the opportunity to collect rewards, similar to results with somatic basal forebrain cholinergic neuron photostimulation (Figure 1).

Concurrent photostimulation of cholinergic terminals and local ACh measurement in the BLA reveals that levels of photo-elicited ACh do not change when associated with reward

Why should photostimulation of cholinergic basal forebrain neurons lead to conditioned responding when associated with reinforcement, but not when unassociated? We postulated that either 1) reinforcement potentiates the amount of ACh released with photostimulation (a “presynaptic” explanation) or 2) the amount of ACh released by photostimulation does not change, but the effects on downstream neurons are modified by reinforcement (a “postsynaptic” explanation). In order to determine whether the amount of ACh released by photostimulation changes as a result of pairing with reinforcement, we measured local ACh in the BLA while concurrently photostimulating basal forebrain cholinergic terminals (Figure 5D). We placed an optic fiber over the BLA in order to use orange light (589 nm) to transiently photostimulate basal forebrain cholinergic terminals using a Cre-dependent, red-shifted optogenetic protein (ChrimsonR) expressed in the basal forebrain of ChAT::Cre mice. We concurrently shined blue light (470 nm) through the same optic fiber to measure local ACh levels using a genetically-encoded ACh sensor in BLA neurons. Sample recordings demonstrated that ACh sensor fluorescence increased during photostimulation only in mice expressing ChrimsonR (Figure 5E), but not in those expressing a control fluorophore (tdTomato, Figure 5F).

We compared, in the same mice, BLA levels of ACh fluorescence during photostimulation during Photostim-Unreinforced and Photostim-Reinforced sessions (Figure 5G-I). Photostimulation elicited robust responses in mice expressing ChrimsonR, but not in mice expressing a control fluorophore (Figure 5G). The amount of measured fluorescence did not depend upon whether photostimulation was provided in Photostim-Unreinforced or Photostim-Reinforced sessions. Taken together with our previous finding that photostimulation of cholinergic terminals in the BLA selectively elevated licking during Photostim-Reinforced

sessions (Figure 5C), our observation that BLA ACh levels did not change with reward suggests that reward associations may gate post-synaptic responses to photostimulation, rather than pre-synaptically changing ACh release.

Lastly in these experiments, given that even briefer photostimulation had been capable of promoting conditioned responding (Figure 1J-K), we additionally performed recordings during a Photostim-Reinforced session, in which photostimulation was provided at various numbers of laser pulses at the same duty cycle. The amount of ACh sensor fluorescence evoked by 1-2 laser pulses, which had been sufficient to promote conditioned responding when photostimulation was targeted to the soma (Figure 1), was similar to levels of ACh at the time of reward delivery in the absence of any photostimulation (Figure S5). Therefore, a level of optogenetically induced ACh release similar to physiologic release can promote conditioned responding, specifically when paired with the opportunity to collect rewards (Photostim-Reinforced sessions).

Cholinergic effects in vivo differ between target regions and depend upon reinforcer context in the amygdala

Because reinforcement context did not change the photostimulation elicited presynaptic release of ACh but led to increased conditioned responding, we next evaluated whether photostimulation effects on target regions involved in conditioned responding might depend on reinforcer context. The BLA and dorsomedial prefrontal cortex (dmPFC) are both involved in conditioned behavior **(Cardinal et al., 2002)**, receive projections from basal forebrain cholinergic neurons **(Kitt et al., 1994; Woolf et al., 1984)**, and are functionally interrelated **(Burgos-Robles et al., 2017; Likhtik et al., 2014, 2005)**. We therefore studied how photostimulation of basal forebrain cholinergic neurons affects in vivo neural activity in these target regions (Figure 6). We again performed surgery on mice to express either ChR2 or a control fluorophore (eYFP) in basal forebrain cholinergic neurons, using Cre-dependent targeting (Figure 6A). In addition to implanting optic fibers over the basal forebrain to photostimulate basal forebrain cholinergic neurons, we also implanted microwire bundles in the dmPFC and BLA to record single unit activity in vivo during photostimulation.

During photostimulation of basal forebrain cholinergic neurons, dmPFC neural activity increased overall across the population (Figure 6B, left; Figure S6). The increase in dmPFC population neural activity during photostimulation was similar for both Photostim-Unreinforced sessions (purple), and Photostim-Reinforced sessions (green). In contrast to the dmPFC, the effects of photostimulation of basal forebrain cholinergic neurons on BLA neural activity differed depending on the session (Figure 6B, right). In Photostim-Unreinforced sessions (purple), the overall BLA population response consisted of facilitation, particularly at onset, whereas in the Photostim-Reinforced sessions (green), the BLA population response had a more striking and sustained suppression. The difference in the BLA population response between the two sessions was evident as early as 135 ms after photostimulation onset and occurred with even shorter durations of photostimulation (Figure S7). There were minimal changes related to photostimulation in control mice expressing eYFP, for both Photostim-Unreinforced and Paired session types (Figure S8).

The population neural responses in the dmPFC and BLA reflected a mix of individual neurons that were facilitated or suppressed by cholinergic basal forebrain photostimulation (Figure 6D-E). In the dmPFC, the proportion of neurons facilitated and suppressed by photostimulation

were stable across session types (Figure 6F, left). In the BLA, however, the proportion of individual neurons that were facilitated tended to decrease during Photostim-Reinforced sessions, and the proportion of neurons that were suppressed increased during Photostim-Reinforced sessions (Figure 6F, right). Comparing between these regions (Figure 6G), a higher proportion of BLA neurons were suppressed than dmPFC neurons during both session types, but a lower proportion of BLA neurons than dmPFC neurons were facilitated during the Photostim-Reinforced sessions. These findings suggested that cholinergic effects in vivo differ between target regions and depend upon reinforcer context in the amygdala.

There was a striking heterogeneity of neural responses within each target region, with some neurons in each region facilitated and others suppressed. We therefore explored how neurons that were facilitated or suppressed might differ. Neurons in the dmPFC that were facilitated by photostimulation of cholinergic basal forebrain neurons during the Photostim-Reinforced sessions had higher baseline firing rates than neurons that were suppressed (Figure S9). There was a possible similar trend in the BLA ($p=0.057$ after correction for multiple comparisons) — neurons that were facilitated during the Photostim-Reinforced sessions had higher baseline firing rates, while neurons that were suppressed had lower baseline firing rates. The possible differences in firing rates suggested that different neurons might be facilitated or suppressed. To identify specific neural subpopulations of BLA neurons that might differentially respond to photostimulation of cholinergic basal forebrain neurons, we transitioned to an ex vivo preparation.

Cholinergic afferents suppress basolateral amygdala output through multiple, molecularly specific pathways ex vivo

We used an ex vivo preparation to determine unambiguously which types of BLA neurons are facilitated or suppressed by photostimulation of cholinergic basal forebrain neurons. We performed surgeries to fluorescently label two populations of BLA neurons to record their post-synaptic responses to photostimulation of basal forebrain cholinergic terminals (Figure 7A). Specifically, we investigated GABAergic neurons that are putative local interneurons, and compared them to projector neurons (in this case those that project to mPFC), which are putative glutamatergic neurons. We used double-transgenic mice (ChAT::Cre x VGAT::flpo) to photostimulate basal forebrain cholinergic axonal terminals in the BLA, through Cre-dependent expression of ChR2. We additionally fluorescently labeled BLA GABAergic neurons by flpo-dependent expression of eYFP. After at least 6 weeks, we performed a second surgery to fluorescently label BLA neurons projecting to the medial prefrontal cortex (mPFC) through injection of a retrograde tracer (cholera toxin b subunit fused to Alexa-647, CTB-647) in the mPFC. One week after the second surgery, mice were euthanized and coronal slices of the BLA were prepared in order to perform whole-cell recordings from either fluorescently identified mPFC projecting BLA neurons (BLA-mPFC) or GABAergic VGAT::flpo BLA neurons (BLA^{GABA}), while photostimulating basal forebrain cholinergic axonal terminals (Figure 7B-C).

These two BLA neural populations were non-overlapping and had strikingly different responses to photostimulation of cholinergic axonal terminals. BLA-mPFC neurons responded to cholinergic terminal photostimulation with a prolonged suppression (Figure 7E-F, Figure S10). In contrast, BLA^{GABA} neurons responded to cholinergic photostimulation with a rapid and more transient facilitation. The amplitude of the fast excitatory postsynaptic potential (EPSP) was greater in BLA^{GABA} neurons compared with BLA-mPFC neurons, while the inhibitory

postsynaptic current (IPSP) amplitude was greater in BLA-mPFC neurons relative to BLA^{GABA} (Figure 7G). These represented independent, direct monosynaptic responses to photostimulation of cholinergic afferents, as each response persisted in the absence of spike-driven synaptic release (to eliminate indirect/polysynaptic transmission), blocked by tetrodotoxin (TTX) (Figure 7H-I).

To understand how these neural populations could have such divergent responses to basal forebrain cholinergic inputs, we tested whether suppression in BLA-mPFC neurons and facilitation in BLA^{GABA} neurons were regulated by different cholinergic receptor classes. Photostimulation evoked IPSPs in BLA-mPFC neurons were blocked by a muscarinic antagonist, but not nicotinic antagonist (Figure 7J, top row). In contrast, the photostimulation evoked facilitation in BLA^{GABA} neurons was blocked by a nicotinic antagonist, but not a muscarinic antagonist (Figure 7J, bottom row). These results suggest a circuit model in which cholinergic afferents suppress BLA output through multiple, molecularly-specific pathways, both through direct muscarinic suppression of projection neurons, as well as through nicotinic facilitation of GABAergic neurons, which can locally inhibit BLA projection neurons (Lee and Kim, 2019; Woodruff and Sah, 2007) (Figure 7K). In total, the effects of cholinergic input to the BLA appear to be a suppression of BLA projector neuron output, and this effect may be most prominent when the system is primed to respond to cholinergic input by behavioral reinforcement.

Discussion

Basal forebrain cholinergic neurons can promote conditioned responding in the absence of discrete cues

Here we demonstrate that photostimulation of basal forebrain cholinergic neurons can promote conditioned responding, even in the absence of discrete external cues. ACh has long been posited to play an important role in directing attention to extrinsic stimuli, as measured by facilitating conditioned responses to such stimuli (Parikh et al., 2007; Pinto et al., 2013). Surprisingly, we observed that photostimulation of cholinergic basal forebrain neurons was sufficient to promote conditioned responding, even in the absence of other discrete stimuli (Figure 1). We observed direct behavioral (Figure 1) and neural responses (Figure 6), often used as readouts of attention, to photostimulation of basal forebrain cholinergic neurons.

Reward availability modulates the impact of basal forebrain cholinergic neurons

Remarkably, photostimulation of basal forebrain cholinergic neurons only drove conditioned responding when paired with the opportunity to collect rewards (Figure 1). Basal forebrain neurons, including cholinergic neurons, are active at the time of both positively and negatively valenced reinforcers (Hangya et al., 2015; Harrison et al., 2016; Peck and Salzman, 2014). Our results demonstrate that at least some part of the previously described reward associations may be due to reward collection behavior such as licking, rather than only reward per se. Previous work has also suggested that ACh may amplify the effects of reinforcers during learning and strengthen plasticity (Jiang et al., 2016). In the current study, reward availability modified the behavioral and neural effects of basal forebrain cholinergic neuron photostimulation itself. BLA neurons became more suppressed as a population (Figure 6), appearing to become more similar to findings in an *ex vivo* preparation from behaviorally naïve animals (Figure 7). Taken together, these data suggest a model wherein effects of ACh may be unmasked or amplified by reward availability.

The effects of basal forebrain cholinergic neurons may be dynamically gated post-synaptically

Given the modulation of ACh effects by reward availability, we investigated whether this difference was due to a difference in the amount of ACh elicited by photostimulation. Cholinergic terminals can express presynaptic receptors, including cholinergic receptors, which may modulate ACh release (Muller et al., 2016; Thany and Tricoire-Leignel, 2011). If photostimulation induced a different amount of ACh release during Photostim-Reinforced sessions, this may have explained the change in conditioned behavior. However, photostimulation of cholinergic terminals in the BLA evoked similar levels of ACh in Photostim-Unreinforced and Photostim-Reinforced sessions (Figure 5). This suggests that the similar levels of ACh instead may have been gated or differentially interpreted by downstream, post-synaptic neurons, depending on reward availability. The postulation of such gating merits future investigation, but may be mediated by coincident signals of reinforcement to the BLA, such as dopaminergic inputs (Lutas et al., 2022, 2019; Tye et al., 2010), given that dopaminergic receptors are expressed by BLA neurons that also express cholinergic receptors (Równiak et al., 2017). Although dmPFC neurons were responsive to photostimulation of basal forebrain cholinergic neurons, these responses did not appear to be dependent on the association

between photostimulation with reward, despite the robust gating effects of dopamine in dmPFC (Vander Weele et al., 2018).

Basal forebrain cholinergic neurons reflect a transition from conditioned stimulus to response

Rather than changing how other stimuli are processed from neutral into conditioned stimuli, our results suggest that cholinergic activity can itself become conditioned. The lack of response to photostimulation during Photostim-Unreinforced Sessions provides important constraints on possible interpretations (Figure 1). Mice were in a familiar context wherein the only meaningful behavioral response was to lick for unpredictable rewards. However, photostimulation of basal forebrain cholinergic neurons during Photostim-Unreinforced sessions did not promote conditioned responding in these sessions, as might be predicted by a number of alternative interpretations, such as nonspecific increases in movement, arousal, or contextual awareness.

Our findings suggest that photostimulated release of ACh can have a similar function as conditioned stimuli or cues, able to trigger conditioned responses. Recent work has shown that basal forebrain cholinergic neurons are active following presentation of conditioned stimuli (Crouse et al., 2020; Guo et al., 2019; Sturgill et al., 2020). Additionally, work in visual cortex has suggested that ACh may help link stimuli with the time of expected rewards (Chubykin et al., 2013; Liu et al., 2015). We also demonstrated, however, that cholinergic neurons were consistently active at the times of conditioned responding, even in the absence of cues and rewards. This suggests that cholinergic transients are poised to play a role in conditioned responding and serve to signal more than just a salient event promoting a response. Indeed, blocking cholinergic muscarinic receptors impaired the ability of mice to respond even to conditioned tones (Figure 2). This is consistent with other studies in which inhibition of cholinergic terminals in the BLA prevented mice from expressing freezing behavior at the time of fear conditioning (Jiang et al., 2016).

Our observation on the impact of ACh on conditioned behavior also provides new context for interpreting several prior results that have examined the role of basal forebrain cholinergic neurons in attention to external stimuli. Interestingly, even when photostimulation of cholinergic basal forebrain neurons has previously been noted to increase discriminability between stimuli, it appears to do this primarily by increasing conditioned responses to conditioned stimuli, rather than suppressing false alarms (Pinto et al., 2013). Additionally, in sustained attention tasks to report the presence of stimuli to collect rewards, photostimulation of basal forebrain cholinergic neurons promote conditioned responding as if cues are present, even in their absence (Gritton et al., 2016), and immunotoxic lesions of basal forebrain cholinergic neurons lead to omissions of any response at all (McGaughy et al., 2002).

The responses of cholinergic basal forebrain neurons (Figure 3) and ACh release within the BLA (Figures 4 and 5) indicate that conditioned responses of licking are represented by cholinergic signaling even in the absence of conditioned stimuli or reward delivery, reminiscent of signals seen in lateral hypothalamic (LH) neurons projecting to the ventral tegmental area (VTA) (Nieh et al., 2015). While LH-VTA neurons were capable of promoting compulsive sucrose seeking behavior, we do not observe the same stereotyped motor sequences in cholinergic neurons as when disinhibiting VTA dopamine neurons via the LH-VTA pathway (Nieh et al., 2016), and the ability of cholinergic signaling to promote compulsivity begs further exploration.

Comparisons to other studies of photostimulation of cholinergic basal forebrain neurons

Cholinergic neurons from the basal forebrain have different projections depend on their location in the basal forebrain (Zaborszky et al., 2012), and even within regions may be physiologically heterogeneous (Laszlovszky et al., 2020). While photostimulation of anterior basal forebrain cholinergic neurons projecting to the lateral hypothalamus suppresses appetite (Herman et al., 2016), here, photostimulation of the more posterior cholinergic population in the sublenticular substantia innominata/extended amygdala increased consummatory behavior (Figure 1). We did not observe an effect on locomotion, in both an unrewarded and a rewarded context, despite the physiologic correlation of cholinergic neuron activity with locomotion (Harrison et al., 2016).

Additionally, while other work has suggested that photostimulation of basal forebrain cholinergic axonal terminals in the BLA can be rewarding (Aitta-Aho et al., 2018), we did not observe a reinforcing effect of somatic basal forebrain cholinergic photostimulation. In addition to differences in the site of photostimulation, we transfected a more posterior and lateral portion of the basal forebrain (+0.05mm AP in Aitta-Aho et al. vs -0.4mm AP here, and ±1.15mm ML in Aitta-Aho et al. vs ±1.80mm here). This more anterior portion of the basal forebrain, closer to the horizontal limb of the diagonal band of Broca (HDB), is more responsive to reward omission, more accurately classifies behavioral outcomes, and more closely tracks fluctuations in pupil-indexed global brain state (Robert et al., 2021). In contrast, cholinergic neurons in the more posterior portions of the basal forebrain are more responsive to unconditioned auditory stimuli, orofacial movements, aversive reinforcement, and showed robust associative plasticity for punishment-predicting cues (Robert et al., 2021).

While it is possible that some of the effects of photostimulation of cholinergic terminals within the BLA were mediated by backfiring of cholinergic axons, several lines of evidence suggest that basal forebrain-BLA cholinergic projection is a relatively distinct population from basal forebrain cholinergic neurons projecting more widely to cortex: 1. Basal forebrain cholinergic neurons that project to the BLA develop earlier embryologically than those that project to cortex and hippocampus (Allaway et al., 2020). 2. Basal forebrain cholinergic neurons that project to the BLA rarely have collaterals (Carlsen et al., 1985). 3. Basal forebrain cholinergic neurons that project to the BLA are sensitive to different immunotoxins and neurotoxins than cholinergic neurons that project to cortex and hippocampus (Beninger et al., 2001; Boegman et al., 1992; Heckers et al., 1994; Heckers and Mesulam, 1994). This suggests that backfiring from cholinergic axons in the BLA to the soma and then to cortex is likely to be limited.

Cell type specific responses to ACh

We noted heterogeneous responses among BLA neurons *in vivo* to photostimulation of basal forebrain cholinergic neurons (Figure 6). Heterogeneous responses have also been previously noted *ex vivo* (Unal et al., 2015; Washburn and Moises, 1992). Through a double transgenic approach, we determined that these heterogeneous responses could be explained on a cellular level, with projecting, putative glutamatergic neurons suppressed, and GABAergic, putative local interneurons neurons facilitated by cholinergic inputs (Figure 7). The BLA GABAergic neuron population is thought to represent local interneurons that inhibit projection neurons (Washburn and Moises, 1992). Although both excitation of GABAergic neurons and inhibition of mPFC projection neurons were monosynaptic, these cholinergic effects could in concert function to suppress BLA output (Lee and Kim, 2019; Pidoplichko et al., 2013; Zhu et al., 2005), which may

decouple regions downstream from the BLA, such as the dmPFC, and allow them to function independently with regards to cholinergic input or other inputs.

This cellular specificity was mediated by different receptors, with short-latency facilitation in GABAergic neurons mediated by nicotinic receptors and longer-latency suppression in projection neurons mediated by muscarinic receptors (Figure 7). Prior histological work had suggested that M1 muscarinic receptors are predominantly expressed by pyramidal neurons in the BLA (McDonald and Mascagni, 2010), and interneurons express nicotinic receptors (Pidoplichko et al., 2013). Functional differences similar to those we have observed between excitatory and inhibitory neurons have been seen in somatosensory cortex (Dasgupta et al., 2018). Strikingly, the behavioral response to even brief photostimulation of basal forebrain cholinergic neurons occurred by approximately 0.5 sec (Figure 1). Surprisingly, this sub-second response appeared primarily mediated by slower muscarinic receptors rather than faster nicotinic receptors (Figure 2). It is possible that these mechanisms might differ based on additional cholinergic factors, such as local interneurons in sensory cortex as well as behavioral context such as reward vs. shock conditioning (Letzkus et al., 2011). Our pharmacology experiments suggest that the effects of basal forebrain cholinergic neurons on nicotinic receptors are insufficient to trigger conditioned responding, although it is possible that we did not block all types of nicotinic receptors. Projection neurons, which receive a preponderance of cholinergic input (McDonald et al., 2011), may serve as a critical point of convergence for ACh influence over BLA networks.

The effects of augmenting ACh levels may depend on context

Multiple mental health disorders involve cholinergic deficiency, including delirium, schizophrenia, and attention deficit hyperactivity disorder (Higley and Picciotto, 2014; Hshieh et al., 2008; Potter et al., 2014). Each of these disorders is associated with severe cognitive and functional impairments (American Psychiatric Association, 2013), symptoms that impact not only patients (Morandi et al., 2015a), but also their families and caregivers (Morandi et al., 2015b; O'Malley et al., 2008). Disappointingly, current strategies to augment cholinergic function, such as cholinesterase inhibitors, have not had a strong clinical impact on several neuropsychiatric illnesses such as dementia, delirium, schizophrenia, and ADHD, because of both insufficient benefit and significant side effects (Biederman et al., 2006; Cubo et al., 2008; Siddiqi et al., 2016; Singh et al., 2012). While there are many reasons that cholinergic augmentation is unlikely to treat any of these complex diseases completely, our translationally motivated concern is that augmenting cholinergic levels, even with temporal and spatial specificity here through optogenetics, may have unpredictable effects depending upon the reward context surrounding this augmentation. Additionally, it is possible that extrinsic augmentation of cholinergic tone may be processed differently than intrinsic fluctuations in cholinergic tone. It is possible that coupling cholinergic augmentation with other therapies, such as cognitive or behavioral therapies, that can explicitly incorporate rewards or proxies for reinforcers, may provide a new opportunity for more sustained and predictable benefits to patients.

Methods

REAGENT or RESOURCE	SOURCE	IDENTIFIER
Experimental Models: Organisms/Strains		
Mouse: B6N.ChAT-IRES-Cre	Jackson Laboratory	IMSR_JAX_018957
Mouse: C57BL/6NJ	Jackson Laboratory	IMSR_JAX_005304
Viruses		
AAV5/EF1a-DIO-hChR2(H134R)-eYFP	UNC Vector Core	AV4313X
AAV5/EF1a-DIO-eYFP	UNC Vector Core	AV4310G
AAVDJ/EF1a-DIO-GCaMP6s	Stanford Vector Core	2612
AAV5/Syn-FLEX-rc[ChrimsonR-tdTomato]	Addgene	62723-AAV5
AAV1/CAG-FLEX-tdTomato	UNC Vector Core	AAV-CAG-FLEX-tdTomato
AAV9/hSyn-Ach4.3 (h-A06)	ViGene	h-A06
Chemicals, Peptides, and Recombinant Proteins		
Tetrodotoxin	Tocris	4368-28-9
4-Aminopyridine	Sigma Aldrich	504-24-5
Scopolamine	Sigma Aldrich	S0929-1G
Mecamylamine hydrochloride	Sigma Aldrich	M9020-5MG
Methyllycaconitine citrate salt	Sigma Aldrich	M168-5MG
Dihydro-ß-erythroidine	Tocris	2349
VECTASHIELD HardSet Antifade Mounting Medium with DAPI	VectorLabs	H-1500
Donkey Anti-Goat IgG Antibody (DyLight 405)	Jackson ImmunoResearch	705-475-147
Donkey Anti-Chicken IgY Antibody (Alexa Fluor 647)	Jackson ImmunoResearch	703-605-155

AB144 Anti-Choline Acetyltransferase Antibody	EMD Millipore	AB144P-1ML
Buprenorphine hydrochloride	MIT Veterinary Pharmacy	NDC 12496-0757-5
C&B Metabond Quick Adhesive Cement System	Parkell	S380
Ortho-Jet BCA Liquid	Lang	B1303
Software and Algorithms		
MATLAB	Mathworks	https://www.mathworks.com/
R	R Foundation for Statistical Computing	http://www.R-project.org/
Adobe Illustrator	Adobe	https://www.adobe.com/products/illustrator.html
Offline Sorter	Plexon	https://plexon.com/products/offline-sorter/
Ethovision XT	Noldus	https://www.noldus.com/ethovision-xt
pClamp 10.4 software	Molecular Devices,	https://www.moleculardevices.com/products/axon-patch-clamp-system/acquisition-and-analysis-software/pclamp-software-suite
Other		
Optic fiber	Thor Labs	TS1843490
Ferrules	Kientec Systems	FSS-LC-330
Small animal stereotaxic frame	David Kopf Instruments	Model 942
USB cameras	ELP	ELP-USBFHD01M-RL36
0.10 mL Microsyringe	World Precision Instruments	NANOFIL-NF33BL-2
Microsyringe Pump UMP3 and Controller Micro4	World Precision Instruments	UMP3-3
Peristaltic pump for ex vivo recordings	Minipuls 3 Gilson	F155001
Miniature Inert Liquid Solenoid Valve	Parker Hannifin	003-0218-900

ATmega328 Arduino	Digi-Key Electronics	1050-1001-ND
Speaker	Digi-Key Electronics	GF0401M-ND
Laser Shutter Heads	Stanford Research Systems	SR475
Rotary Encoder	US Digital	E2-200-250-NE-D-D-B
Multifunction I/O Device	National Instruments	USB-6211
Pulse stimulator	A.M.P.I.	Master-8
5mm White LED	Digi-Key Electronics	C513A-WSN-CY0Z0341-ND
Electrodes: 22.9-µm nichrome wire	California Fine Wire	Stablohm 675
Gold Non-Cyanide	Sifco asc	80535500
Open Ephys Acquisition Board	Open Ephys	C3324
HM430 Microtome	Thermo Fisher Scientific	910010
Confocal Laser-Scanning microscope	Olympus	FV1000
Diode Blue 473 nm Laser	OptoEngine LLC	MBL-III-473/ 1~100mW
Horizontal puller for glass microelectrodes for *ex vivo* recordings	Sutter	P-1000
Multiclamp amplifier for *ex vivo* recordings	Molecular Devices	700B
Microscope for *ex vivo* recordings	Olympus	BX51

Subjects

Female and male hemizygous ChAT::Cre mice (Chen et al., 2018; Rossi et al., 2011) were group housed by sex until surgery on a reversed 12-hour light-dark cycle in a humidity and temperature controlled vivarium. All behavioral experiments were conducted during the dark phase of the animals' cycle. All experiments involving the use of animals were in accordance with National Institutes of Health guidelines and approved by the Massachusetts Institute of Technology's Committee on Animal Care.

General Stereotaxic Surgery Methods

General surgical methods are provided here and specific subject/surgery details for each experiment are detailed in their respective sections below. Surgeries were performed prior to behavioral training and all other experiments. For all mice, surgeries were performed under aseptic conditions and body temperature was maintained with a heating pad. Mice were anesthetized with isoflurane in oxygen (4% for induction, 1-2% for maintenance, 0.8 L/min oxygen flow rate). Following induction, we shaved the scalp and placed the subjects on a digital small animal stereotaxic instrument (David Kopf Instruments). Ophthalmic ointment was applied to the eyes and the incision area was scrubbed three times with alternating betadine and 70% ethanol. An incision was made along the midline to expose the skull, which was then leveled. All measurements for virus injections and implants were made relative to Bregma using the approximated intersection of skull sutures. A dental drill was used to perform small craniotomies (EXL-M40, Osada).

Viral injections were performed using a beveled 33-gauge microinjection needle connected to a 10 µL microsyringe (Nanofil; WPI, Sarasota, FL, USA) at a rate of 100 nL/min using a microsyringe pump (UMP3; WPI) and pump controller (Micro4; WPI). After injections were complete, ten minutes were allowed to pass before the needle was slowly withdrawn. Optic fibers and/or electrodes were then implanted. For head-fixation, a 2mm x 2mm x 25mm aluminum headbar was placed horizontally over Lambda. A layer of adhesive cement (C&B Metabond; Parkell Inc., NY, USA) was used to secure the implants and headbar to the skull, followed by a black cranioplastic cement (Ortho-Jet; Lang, IL, USA) to prevent light escape. The cement was allowed to dry completely before closure of the incision with 4.0 nylon sutures.

Subjects received a perioperative subcutaneous injection of sustained release buprenorphine (1 mg/kg) for analgesia. During recovery, subjects were also injected subcutaneously with 1ml of warm Lactated Ringers solution and kept on a heat pad until fully recovered from anesthesia. For all experiments involving viral or tracer injections, animals containing mistargeted injections were excluded after histological verification.

Stereotaxic Surgery for Optogenetic Photostimulation of Basal Forebrain Cholinergic Neurons

For optogenetic photostimulation of basal forebrain cholinergic neurons, 500 nL of an adeno-associated virus encoding either channelrhodopsin (AAV5/EF1a-DIO-hChR2(H134R)-eYFP; UNC, 5.5 x 10^{12}) or a control fluorophore (AAV5/EF1a-DIO-eYFP; UNC, 4.4 x 10^{12}) were injected bilaterally into basal forebrain of each hemisphere at AP -0.4, ML ±1.8, DV -4.7. For photostimulation of cholinergic neurons at their basal forebrain soma, optic fibers (300µm diameter) were implanted bilaterally into the basal forebrain at AP -0.4, ML ±1.8, DV -4.3. For photostimulation of cholinergic neuron axon terminals in the BLA, optic fibers (300µm diameter) were implanted unilaterally above the BLA at AP -1.4, ML ±3.1, DV -4.6.

Head-fixed Behavioral and Optogenetic Equipment

Head-fixed boxes were custom built using various optomechanical components (ThorLabs) and 3D printed parts mounted on top of a solid aluminum optical breadboard (SAB0810, Base Optics) housed within a 19-quart drybox (UC19-YHV, Engel Coolers). Mice were head-fixed on either a 3D printed rectangular platform, or a custom 3D printed linear-belt treadmill, in front of a blunt 18G needle spout (75165A754, McMaster Carr). For electrophysiology experiments, licks

were registered using an infra-red beam passing in front of the spout tip (emitter 935 nm, OP165A, TT Electronics/Optek Technology; phototransistor SFH 309 FA-4/5, OSRAM Opto Semiconductors). For other experiments, licks were registered using a capacitive contact circuit (MPR121, Adafruit) that was interpreted by a microcontroller (Arduino Uno SMD R3 ATMEGA328, Arduino). A white LED module (1621, Adafruit) provided a low level of ambient light.

Behavioral System Control

All behavior for each box was controlled by a microcontroller (Arduino Mega 2560 Rev3, Arduino), which ran customized behavioral code to register licks, deliver fluid, present tones, and trigger photostimulation. Fluid rewards consisted of 4µL of a sweet caloric fluid (Vanilla Ensure Original Shake, Abbott). Fluid delivery was controlled by opening a solenoid valve (003-0860-900, Parker, NH, USA) and delivered to the spout by gravity flow via plastic acrylic tubing (McMaster-Carr, IL, USA). All valves were calibrated using timing duration to ensure consistent fluid volumes.

Head-fixed Behavioral Training

After at least 3 weeks of recovery from surgery, animals were food restricted and maintained on at least 85% body weight. Animals had free access to water. After stable food restriction, training was initiated. On each day, mice received enough food supplementation using standard lab chow to maintain their body weight between 85-90% of their free body weight (typically 2.5-5g).

Handling

Mice were first handled for 5 min a day for 5 days to reduce stress and increase familiarity with the experimenter. During this time, they also were given fluid rewards via a hand held plastic pipette.

Uncued Head-fixed Training

For uncued head-fixed training, mice were head-fixed in the behavioral box and a lickspout was placed close to the mouth. The animal received a few drops of fluid reward, to initiate licking. Once the mouse started licking, the spout was retracted away slightly to a distance still reachable by licking.

Sessions were divided into trials of 3 sec windows with intervening unrewarded intertrial intervals (ITIs). During early training, 90% of the 3 sec windows were designated as *Windows of Opportunity*. If mice licked during the *Windows of Opportunity*, they received a 4 µl fluid reward after a brief delay (0.1 sec). Since rewarded windows were not cued, mice did not know when they initiated a lick whether it would be rewarded, making the rewards unpredictable. Only the first lick within a window resulted in reward delivery. The ITIs between *Windows of Opportunity* were randomly selected from an exponential distribution between 3-6 sec (mean 4 sec). The remaining 10% of 3 sec windows were designated as matched *Unrewarded Windows*. If mice licked during this time, no reward was delivered, similar to the rest of the unrewarded ITIs.

The first session was 30 min long and subsequent sessions were 1 hr long. Mice were trained daily until they attempted to collect rewards on at least 30% of uncued *Windows of Opportunity*, in order to avoid ceiling and floor effects of subsequent manipulations. The likelihood of licking

was defined as percent of 3 sec windows, for either Rewarded or *Unrewarded Windows*, in which mice licked at least once. Mice underwent approximately 7 days of uncued head-fixed training to reach criterion. Single measurements were compared between ChR2 and eYFP mice using rank-sum tests in R (R Core Team, 2015). Repeated measurements from the same mice were analyzed using linear mixed effects models fit by restricted maximum likelihood using the lme4 package (Bates et al., 2015, p. 4). Fixed effects included virus group (ChR2 vs. eYFP) and window type (Rewarded vs. Unrewarded), as well as their interaction. Random effects were modeled using random intercepts for each subject. P values were obtained using the lmerTest package (Kuznetsova et al., 2017).

Optogenetic Photostimulation of Basal Forebrain Cholinergic Neurons during Head-Fixed Behavior

Following initial uncued head-fixed training, ChR2 and eYFP mice were tested to examine whether photostimulation of basal forebrain cholinergic neurons affected licking, the conditioned response. For optogenetic photostimulation, a 473 nm diode laser (MBL-III-473/1~100mW, OptoEngine LLC) was used as a light source. Photostimulation was delivered at 4mW (measured at the fiber tip), using 5 ms pulses delivered at 20 Hz. Lasers were continuously on to minimize power fluctuations, but photostimulation was gated at the source prior to entering a collimator (HPUC-23AF-473-S-11AS-LBH-BL-SP, OZ Optics) through a laser shutter head (SR475, Stanford Research Systems), controlled by a four-channel laser shutter driver (SR474, Stanford Research Systems). Laser light was then routed from the collimator through patch cords (Doric, Québec, Canada) and split for bilateral photostimulation using a rotary joint (1x2 Fiber-optic Rotary Joints - Intensity Division; Doric, Québec, Canada), with a subsequent patch cord terminating on the implanted ferrule. All connections including that to the implanted ferrule were optically shielded to prevent light leakage.

Photostim-Unreinforced Sessions

To assess innate behavioral responses to photostimulation of basal forebrain cholinergic neurons, mice underwent one session in which they received photostimulation of cholinergic basal forebrain neurons during unrewarded ITIs (Photostim-Unreinforced sessions). On a subset of ITIs, approximately once a minute, photostimulation was delivered for 2 sec, and the likelihood and latency of licking was recorded in the 3 sec following photostimulation onset to assess effects on conditioned responding.

During this session, if mice licked during unsignaled *Windows of Opportunity*, which did not have photostimulation, they continued to receive rewards. ITIs between *Windows of Opportunity* were randomly selected from an exponential distribution between 4.5-10 sec (mean 5 sec). Licking during ITIs had no consequence, which included photostimulation during these sessions. Photostimulation was delivered at least 3.5 sec away from either the beginning or end of a *Window of Opportunity*.

Photostim-Reinforced Sessions

During Photostim-Reinforced sessions, 2 sec of photostimulation was now delivered starting at the onset of the 3 sec *Windows of Opportunity*. Photostimulation was delivered only on a subset of *Windows of Opportunity* (15%). Approximately one photostimulation trial was delivered per minute, thereby making up the minority of total session time and a minority of *Windows of*

Opportunity. Licking during *Windows of Opportunity* yielded a fluid reward, whether the mouse received photostimulation or not.

Mice ran on two Photostim-Reinforced sessions, and behavior was analyzed from the second session, based on a priori planning in order to minimize multiple post-hoc comparisons. Data from the planned analysis is shown in Figure 1, with data from all sessions in Figure S2. We analyzed data using linear mixed effects models, given the repeated measures from mice. Fixed effects included Virus (ChR2 vs. eYFP), Photostimulation trial types (Photostim vs. No photostim), and Reinforcement Session type (Photostim-Reinforced vs. Photostim-Unreinforced), as well as first and second order interactions. Random effects were modeled using random intercepts for each subject. Post-hoc tests for all linear mixed effects models were performed using the emmeans package (Lenth, 2020), with the Kenward-Roger method for degrees-of-freedom, and the Sidak method for p value adjustment for multiple comparisons.

During a subsequent session, we varied photostimulation parameters to assess how little or brief the stimulation needed to be to produce conditioned responding. We randomly delivered photostimulation on *Windows of Opportunity* using either 1, 2, or 10 pulses of light at 20 Hz, corresponding to up to 0.5 sec of photostimulation. These continued to be delivered at the onset of 3 sec *Windows of Opportunity*. Fixed effects for linear mixed effects model analysis included Virus (ChR2 vs. eYFP), photostimulation pulses (0, 1, 2, 10), and their interaction. Random effects were modeled using random intercepts for each subject. Post-hoc tests corrected for multiple comparisons included comparisons between ChR2 and eYFP at each number of pulses, and comparisons within each virus group for 1, 2, or 10 pulses to 0 pulses.

Treadmill

To assess the effects of basal forebrain photostimulation on locomotion, we collected locomotion data from a custom-made linear belt treadmill in the head-fix setup. Locomotion data was collected using a rotary encoder (US Digital E2-200-250-NE-D-D-B), digitized using a NI-USB-6211 at 1kHz and analyzed using MATLAB. There was no behavioral consequence of running. Behavioral event timings, including trial onset, photostimulation, licking, and reward delivery, were synchronized by sending TTLs from the Arduino microcontroller into an R-2R resistor ladder to multiplex the events into a single analog input channel on the NI-USB-6211.

Treadmill locomotion was analyzed around photostimulation, starting 2 sec before photostimulation onset until 4 sec after. Photostimulation duration was 2 sec. Data was binned in 0.1 sec bins for peri-event time histograms. Each bin was compared between ChR2 and eYFP mice for each session type (Photostim-Unreinforced or Photostim-Reinforced). Statistical significance of each bin was tested between groups using rank-sum tests, $p < 0.01$. To compare photostimulation evoked locomotion between sessions for the same mice and between groups, we used linear mixed effects models to analyze the mean locomotion during photostimulation (0 - 2 sec). Fixed effects included Virus (ChR2 vs. eYFP), Reinforcement Session type (Photostim-Reinforced vs. Photostim-Unreinforced), as well as their interaction. Random effects were modeled using random intercepts for each subject.

Pupillometry

In order to assess changes in arousal, we recorded pupil diameter during behavioral sessions. An infrared USB camera (ELP-USBFHD01M-RL36, ELP) was placed 15cm from the mouse's

eye. The infrared LED/emitter panel was unscrewed and pointed away from the mouse to decrease eye secretions. Ambient light was adjusted to keep the pupil size at an intermediate level, which allowed the pupil to fluctuate over a dynamic range. Recordings were started and stopped at the same time as behavior using Processing 2.2.1 running on a Windows desktop computer (Hewlett-Packard), which also initiated the Arduino microcontroller running behavior. Files were saved at 30 Hz as 640x480 pixel ogg vorbis video files. Behavioral event timings were identified for subsequent synchronization using 940 nm infrared LEDs (IR204, Everlight Electronics, Digi-Key) to signal behavioral events, including trial onset, photostimulation, licking, and reward delivery.

For pupil and body part tracking we used DeepLabCut (version 2.0.8) (Mathis et al., 2018; Nath et al., 2019). We labeled eight points for the right pupil of each mouse, according to cardinal and intercardinal compass directions (North, NorthEast, East, SouthEast, South, SouthWest, West, and NorthWest). Specifically, we labeled 483 frames taken from 25 videos from 21 animals, then 95% were used for training. We used a ResNet-50 based neural network with default parameters for 1.03 million training iterations (He et al., 2016; Insafutdinov et al., 2016). We validated with a single shuffle and found the test error was: 1.08 pixels, train: 1.93 pixels. We then used a p-cutoff of 0.9 to condition the X, Y coordinates for future analysis. This network was then used to analyze videos from similar experimental settings. Relative pupil diameters were determined by calculating the distance for each major axis (North-South, East-West, NorthWest-SouthEast, NorthEast-SouthWest), and then taking the mean of these four measurements.

Pupil diameter was normalized to the diameter prior to photostimulation (-2 to -1 sec relative to photostimulation onset), and the pupil diameter from each frame for each trial was expressed as the percent difference from baseline. Relative pupil diameter changes at each frame were compared between ChR2 and eYFP mice using rank-sum testing ($p<0.05$).

To compare photostimulation evoked pupil diameter changes between sessions for the same mice and between groups, we used linear mixed effects models to analyze the mean pupil diameter following events onsets (0 - 4 sec), separately for photostimulation and for reward delivery. Fixed effects included Virus (ChR2 vs. eYFP), Reinforcement Session type (Photostim-Reinforced vs. Photostim-Unreinforced), as well as their interaction. Random effects were modeled using random intercepts for each subject. Post-hoc tests corrected for multiple comparisons included four comparisons between ChR2 and eYFP for each session, and between sessions for each viral group.

Cued Tone Task

In a separate set of sessions, mice were trained to respond to 3.5kHZ or 12kHz tones (frequencies counterbalanced between mice). Tones were generated using the tone function on the Arduino Mega, passed through analog low and high pass filters, and presented using an 8-ohm speaker (GF0401M, CUI Devices) at 55-60 dBA. Tones were presented for 2 sec and mice were rewarded for licking during the 3 sec response window. These 1 hr sessions included only tone trials to signal rewards opportunities—there were no longer any unsignaled *Windows of Opportunity*.

Interleaved Tone or Photostim-Reinforced Trials Session

After three days of training on the cued tone task, mice were tested on a session which included interleaved tone or Photostim-Reinforced windows. 2 sec of either tone or photostimulation were presented, and mice could receive a reward if they licked within 3 sec of the onsets. Only 90% of lick responses on each trial type were rewarded. Tone and photostimulation trials were equally likely and were separated by ITIs with a mean of 12 sec (range 7-22 sec, exponential distribution). Baseline/ITI licking was assessed by *a priori* statistically identifying 3 sec windows between tone and photostimulation trials, with similar ITIs.

In vivo Cholinergic Antagonist Pharmacology

In order to test which class of receptors mediated the effects of photostimulation of cholinergic basal forebrain neurons, mice were injected with cholinergic receptor antagonists prior to an Interleaved Tone or Photostim-Reinforced Trials Session. Using a 27 gauge needle, we injected mice with either the muscarinic receptor antagonist scopolamine (0.3 or 1 mg/kg) (Chintoh et al., 2003) or the nicotinic receptor antagonist mecamylamine (1mg/kg) (Adermark et al., 2014; Zachariou et al., 2001). These drugs and doses were chosen in discussion with an expert in the field (Dr. Marina Picciotto, personal communications). Injections were made 10 minutes before behavioral sessions. All drugs were dissolved in sterile saline and injected at 10 ml/kg volumes. Sterile saline alone was used for control injections. Drug injection orders were counterbalanced across animals.

We analyzed data using linear mixed effects models, given the repeated measures from mice. Fixed effects included Virus (ChR2 vs. eYFP), Trial types (Tone, Photostim, or ITI), and Drug session type (Saline, Scopolamine 0.3mg/kg, Scopolamine 1mg/kg, Mecamylamine 1mg/kg), as well as first and second order interactions. Random effects were modeled using random intercepts for each subject. Post-hoc tests corrected for multiple comparisons were stratified by sessions, and included comparisons between ChR2 and eYFP for each trial type, and comparisons within each virus group for all three pairs of trial types.

Open Field Test

To assess whether BF cholinergic stimulation had an effect on locomotion, animals underwent an open field test (Matthews et al., 2016). We attached fiber optic patch cables to the implanted ferrules on mice. Mice were then placed in the center of an open 50 x 53 cm arena composed of four transparent Plexiglas walls illuminated by 30 lux ambient light. They were allowed to freely move throughout the arena for 15 min. A video camera was positioned directly above the arena to track the movement of each mouse throughout the session (EthoVision XT, Noldus, Wageningen, Netherlands).

The session was divided into three 5 min windows with photostimulation occurring throughout the middle 5 min window (473 nm light, 4mW, 5 ms pulses at 20 Hz. The same laser and shutter setup described above was used except that a Master-8 pulse stimulator (A.M.P.I., Jerusalem, Israel) interfaced with the EthoVision XT system was used to drive laser pulses. Acetic acid (0.03%) was used to wipe and clean the chamber between animals.

We analyzed data using linear mixed effects models. Fixed effects included Virus (ChR2 vs. eYFP), Laser status (On or Off), and Time by 5min window, as well as the interaction between virus and laser status. Random effects were modeled using random intercepts for each subject.

Real Time Place Preference

To assess whether cholinergic stimulation was inherently reinforcing or pleasurable to the animals, mice underwent a Real Time Place Preference test (RTTP) (Matthews et al., 2016). We attached fiber optic patch cables to the implanted ferrules on mice. Mice were then placed in the center of a transparent Plexiglas chamber (50 x 53 cm) divided into left and right compartments using center dividers, with an open gap in the middle allowing mice to freely access both compartments. The chamber was illuminated with 30 lux ambient light. Mice were allowed to freely move between compartments for 45 minutes during which entry into one of the two sides resulted in continuous photostimulation (473 nm light, 4mW, 5 ms pulses at 20 Hz). The side paired with photostimulation was counterbalanced between animals and activity was averaged across two days. A video camera was placed directly above the arena to track mouse movement (EthoVision XT) and trigger photostimulation. Acetic acid (0.03%) was used to wipe and clean the chamber between animals. The percent of time mice spent on the side on which the laser was ON was averaged over two days, and compared between ChR2 and eYFP mice using a t-test.

GCaMP Photometry of Basal Forebrain Cholinergic Neurons

Stereotaxic Surgery for GCaMP Photometry from Basal Forebrain Cholinergic Neurons

To measure neural activity from basal forebrain cholinergic neurons, we injected 1000 nL of an adeno-associated virus encoding the genetically-encoded calcium sensor GCaMP (AAVdj/EF1a-DIO-GCaMP6s; Stanford Vector Core) into the basal forebrain of ChAT::Cre mice (AP -0.7; ML ±1.75; DV -5.1 and -4.3, 500 nL at each depth). An optic fiber was implanted over the basal forebrain (AP -0.7; ML 1.75; DV -4.5).

GCaMP Photometry Set-Up

The hardware setup for acquisition of bulk calcium fluorescence from multiple sites was adapted from (Kim et al., 2016). The setup allowed for excitation of the sample at two wavelengths (405 and 470 nm) and collection of fluorescence emission at 525 nm. The excitation path consisted of a 405 nm and a 470 nm LED (Thorlabs M405FP1 and M470F3) which were collimated (Thorlabs F671SMA-405) and coupled to 400 nm and 469 nm excitation filters (Thorlabs FB400-10 and MF469-35), respectively. Compared to 470 nm excitation, 405 nm excitation of GCaMP is closer to the isobestic wavelength for calcium-dependent and calcium-independent GCaMP fluorescence, and thus was used to assess movement- and autofluorescence-related noise. Light from these two excitations sources were combined into one path via dichroic mirrors and filled the back aperture of a 20x air objective (Nikon CFI Plan Apo Lambda). A fiber optic patch cord (Doric) containing optic fibers bundled into a single ferrule (400 µM diameter, 0.48 NA for each fiber) was positioned at the working distance of the objective. The end of the patch cable was connected to implanted ferrules on the animals' head. Emission resulting from the 405 or 470 nm excitation was split by a dichroic mirror, passed through a 525 nm emission filter (Thorlabs MF525- 39), and focused through a tube lens (Thorlabs AC254-100-A-ML) onto the face of CMOS camera (Hamamatsu ORCA-Flash V2). Frames were captured at 40 Hz and each LED was modulated at 20 Hz in an alternating fashion, resulting in a 20 Hz sample rate in the reference (405 nm excitation) and signal (470 nm excitation) channels. LED and camera timing as well as recording of timestamps from behavioral equipment was achieved using a data acquisition board (National Instruments NI BNC-2110). The system was controlled through

custom MATLAB scripts modified from those made available by (Kim et al., 2016). Prior to the start of each session, the entire system was shielded from outside light using blackout cloth.

Behavior during GCaMP Photometry

To investigate whether basal forebrain cholinergic neural activity increased during conditioning responding, mice first underwent uncued head-fixed training. Mice were rewarded for licking during unsignaled 3 sec *Windows of Opportunity*. Rewards were delivered after a 0.5 sec delay from the first lick in a *Window of Opportunity* to account for the slow dynamics of GCaMP6s. Mice were not punished for licking during the unrewarded ITIs.

Following recordings during the uncued stage of training, mice were then transitioned to the Cued Tone task described above. Mice were now rewarded for licking following the onset of tone cues, and rewards were delivered after a 0.5 sec delay from the first lick within 3 sec of tone onset.

Photometry Analysis

Photometry fluorescence traces were filtered using a 60 sec median filter to extract an estimate of baseline fluorescence by accounting for bleaching and low frequency fluctuations. The residual trace was filtered with a 3rd order median filter to eliminate single time point artifacts. DF/F was obtained by taking the difference between the residual trace and the baseline estimate and dividing by the baseline estimate, which was then expressed in percent. Fluorescence levels were compared as the area under the curve in a time window before (-2 to -1.5 sec) and after (0 to 0.5 sec) events. Fixed effects for linear mixed effects model analysis included Wavelength (470 nm signal vs. 405 nm reference), Time point (before or after event), and Event type, and first and second order interactions. Random effects were modeled using random intercepts for each subject. Post-hoc tests corrected for multiple comparisons within each session.

ACh Sensor Measurements

Stereotaxic Surgery for ACh Sensor Measurements

To measure local levels of ACh, we injected 400 nL of an adeno-associated virus encoding the genetically-encoded ACh sensor GACh3.0 (AAV9/hSyn-Ach4.3, ViGene) (Jing et al., 2018) into the BLA (AP -1.4; ML ±3.1; DV -5.2). In order to photostimulate basal forebrain cholinergic terminals projecting to the BLA, an anterograde virus driving expression of the red-shifted opsin ChrimsonR (AAV5/Syn-FLEX-rc[ChrimsonR-tdTomato]) was injected into the basal forebrain (500 nL, AP -0.4; ML ±1.8; DV -4.7). For control mice, a virus encoding just the fluorophore (AAV1/CAG-FLEX-tdTomato), was injected with the same volume at the same coordinates. An optic fiber (400um diameter) was then implanted over the BLA (AP -1.4; ML ± 3.25; DV -4.8), in order to provide optical access to both record GACh3.0 related fluorescence using 470 nm blue light as well as photostimulate basal cholinergic forebrain cholinergic terminals in the BLA using interleaved 589 nm yellow light. Data was analyzed similar to the GCaMP photometry experiments, except that there was only fluorescence data from one channel (470 nm).

Behavior during ACh Sensor Measurements

To investigate whether local ACh levels changed in the BLA during conditioning responding, mice first underwent uncued head-fixed training. Mice were rewarded for licking during

unsignaled 3 sec *Windows of Opportunity*. Rewards were delivered after a brief (0.1 sec) delay from the first lick in a *Window of Opportunity*. Mice were not punished for licking during the unrewarded ITIs.

Similar to optogenetic experiments, mice were then tested during a Photostim-Unreinforced session and two Photostim-Reinforced sessions. Results are presented from the second Photostim-Reinforced session. During a subsequent session, we again varied photostimulation parameters by randomly delivering photostimulation on *Windows of Opportunity* using either one, two, or ten 5 ms pulses at 20 Hz, corresponding to up to 0.5 sec of photostimulation. These pulse trains were also delivered at the onset of 3 sec *Windows of Opportunity*.

Mice were then trained for three sessions on the Cued Tone task described above. Mice were rewarded for licking following the onset of tone cues, and rewards were delivered after a brief (0.1 sec) delay from the first lick within 3 sec from tone onset.

Concurrent Optogenetic Photostimulation and Measurement of Local ACh Levels using a Genetically-encoded Fluorescent Sensor

The hardware setup for acquisition of bulk ACh fluorescence from multiple sites was similar to that for GCaMP photometry. For concurrent optogenetic manipulation experiments, the system was modified to allow for 589 nm yellow light excitation through the same patch cable. An additional dichroic mirror combined the LED light paths with that of a 589 nm laser. The laser was powered on throughout the experiments to minimize intensity fluctuations and was modulated by opening/closing a mechanical laser shutter head (SR475, Stanford Research Systems), controlled by a shutter driver (SR474, Stanford Research Systems). 470 nm LED light was used to excite the ACh sensor, and 525 nm emitted photons were collected, for 25 ms at 20 Hz (every 50 ms) using the filters described above. When photostimulation was provided using 589 nm laser light, it was delivered as 5 ms pulses at 20 Hz (4 mW) in between the 470 nm light pulses, in order to prevent spectral crosstalk.

Fluorescence levels were analyzed as the area under the curve after photostimulation onset (0 to 0.5 sec for reward, 1, 2, or 10 pulses; 0 to 2 sec for 2 sec photostimulation). Fixed effects for linear mixed effects model analysis for sessions with different durations of photostimulation included Virus (ChrimsonR vs. tdTomato control fluorophore), photostimulation pulses (Reward, 1, 2, or 10 pulses), and their interaction. Random effects were modeled using random intercepts for each subject. Post-hoc tests corrected for multiple comparisons included comparisons between ChrimsonR and tdTomato mice at each number of pulses, and comparisons within each virus group for 1, 2, or 10 pulses to Reward. For comparisons of evoked ACh in Photostim-Unreinforced and Photostim-Reinforced sessions, linear mixed effects model fixed effects included Virus (ChrimsonR vs. tdTomato), Session type (unreinforced or reinforced), and their interaction. Random effects were modeled using random intercepts for each subject.

in vivo Electrophysiology

in vivo Electrophysiology Surgery

Mice were anesthetized using isoflurane gas (1-4%) and mounted on a stereotaxic apparatus (Kopf Instruments) to implant optrodes (i.e., combination of electrode and optical fiber). A midline incision was made down the scalp and craniotomies were opened using a dental drill. Optrodes were chronically implanted in either hemisphere in the basolateral amygdala (BLA)

and the prelimbic (PL) subregion of the dorsomedial prefrontal cortex (dmPFC). The stereotaxic coordinates to target the BLA were -1.50 mm anterior-posterior (AP), ±3.15 mm medial-lateral (ML), and -5.00 mm dorsal-ventral (DV). The stereotaxic coordinates to target PL were +1.80 AP, ±0.35 mm ML, and -2.00 mm DV. In addition to these optrodes, optical fibers were implanted bilaterally in the basal forebrain (BF) to photostimulate ChR2-expressing ChAT neurons while recording neural activity from the BLA and dmPFC. The stereotaxic coordinates for the BF fibers were -0.40 mm AP, ±1.80 mm ML, and -4.50 mm DV. All stereotaxic coordinates were calculated relative to Bregma. Finally, an aluminum bar was horizontally positioned behind lambda to provide anchoring points during head-fixed recordings. All these implants were secured to the skull using stainless steel self-drilling screws (Small Parts), adhesive cement (C&B Metabond, Parkell) and dental acrylic (Ortho-Jet, Lang Dental). At the end of the surgeries, incisions were sutured, and postoperative analgesia and fluids were provided as needed. Mice were allowed to recover from surgery for at least one week.

in vivo Electrophysiology Recordings

Extracellular recordings were performed using in-house-built multichannel electrodes, each containing a 16-channel Omnetics connector, an optical fiber attached to the connector, and a low-resistance silver wire to provide ground. The microwire used for the electrodes was a 22.9-µm HML-insulated nichrome wire (Stablohm 675, California Fine Wire). Microwires were secured to the connector pins using a silver print coating (GC Electronics). All connections were then secured using dental acrylic. Serrated fine scissors were used to cut the tip of the microwires to a length of 500-1000 µm from the tip of the optical fiber. The microwire tips were then gold-plated to reduce impedance and improve signal-to-noise ratio (Ferguson et al., 2009). Gold plating was achieved by submerging the electrode tips in a solution containing equal parts of a non-cyanide gold solution (SIFCO Selective Plating) and a 1 mg/mL polyethylene glycol solution. A cathodal current of 1 µA was applied to individual channels to reduce impedances to a range of 200-300 kΩ.

Multichannel extracellular recording setups (Open Ephys) were used to monitor neural activity while mice performed behavioral tasks. Extracellular signals were recorded at 30 kHz with band-pass filters set at 0.2 and 7,600 Hz. These raw signals were then processed offline to extract single-unit activity.

in vivo Electrophysiology Spike Extraction

A common reference was calculated for each 16-channel array, by calculating the median trace across all channels. This trace was then subtracted from each channel on that array. Data was then filtered from 300-7000 Hz using a fourth degree Butterworth filter applied using the filtfilt function in Matlab. Spikes were identified by negative deviations greater than 7.4 times the median absolute deviation. Spikes were aligned to their minima and waveforms from 375µs before the trough and 1000µs after the trough were extracted for spike sorting. Single-unit waveforms were then sorted using commercial software (Offline Sorter, Plexon Inc), by combining principal component and peak-trough voltage features in three-dimensional space. Neural firing properties were visually inspected, including auto-correlations and cross-correlations, in order to exclude multi-unit activity or repeated recordings of the same unit across multiple wires in a bundle. Neurons were additionally inspected to ensure they did not represent behaviorally locked artifacts. Only neurons that fired at least 0.01 Hz across the whole session were included in analyses.

in vivo Electrophysiology Analysis

Peri-event time histograms were constructed by extracting spiking activity around photostimulation in 10 ms bins from 8 sec before to 16 sec after photostimulation onset. Baseline activity was defined as the activity from 4 sec before up to the onset of photostimulation. Activity for each trial was transformed using the mean and standard deviation of baseline activity across trials. Data was smoothed with a 50 ms Gaussian kernel. Activity within each area for each bin was compared using rank-sum tests to compare Photostim-Unreinforced and Photostim-Reinforced sessions, separately for ChR2 and eYFP mice.

Modulation around the time of photostimulation was calculated by comparing firing rates before photostimulation onset (-1 to 0 sec) with firing rates shortly after photostimulation onset (0 to 0.5 sec). Facilitation was classified as neurons with statistically significant increases in firing rates after photostimulation onset, and suppression was defined as neurons with statistically significant decreases in firing rates after photostimulation onset (sign-rank test, $p < 0.01$). Proportions were compared using two-sided Chi-square proportion tests, with p values corrected for multiple comparisons using Holm's procedure.

in vivo Electrophysiology Histology

Mice were anesthetized using isoflurane to mark the position of electrode tips by producing microlesions (anodal current, 25-40 µA for at least 20 s). Mice were then euthanized with sodium pentobarbital (150 mg/kg), and transcardially perfused with saline solution and 4% paraformaldehyde (PFA, pH 7.3). Brains were extracted and fixed in 4%-PFA for at least 24 h and then equilibrated in a 30% sucrose solution for 48 h. Coronal sections were cut at 40 µm using a microtome (HM430, Thermo Fisher Scientific). Brain sections containing the BLA, dmPFC, and BF were mounted on microscope slides, and stained with DAPI (4',6-diamidino-2-phenylindole). Images of the BLA, dmPFC, and BF were acquired using a confocal laser-scanning microscope (Olympus FV1000). Expression of eYFP and/or ChR2 was examined from the BF sections, whereas the location of microlesions was examined from the BLA and dmPFC sections to determine the neural recording sites. These were reconstructed onto coronal drawings adapted from a mouse brain atlas (Franklin, 2008).

ex vivo Electrophysiology

ex vivo Electrophysiology Surgery

We generated double transgenic mice by crossing homozygous ChAT::Cre mice with hemizygous VGAT::flpo mice. Double hemizygous offspring (ChAT::Cre x VGAT::flpo mice), confirmed by genotyping (Transnetyx) were used for these experiments. In a first surgery, for optogenetic photostimulation of basal forebrain cholinergic neurons, we injected 500 nL of an adeno-associated virus encoding channelrhodopsin (AAV5/EF1a-DIO-hChR2(H134R)-mCherry; UNC, 3.5×10^{12}) bilaterally into basal forebrain of each hemisphere at AP -0.4, ML ±1.8, DV -5. For fluorescent labeling of BLA GABAergic neurons, we injected 400 nL of an adeno-associated virus encoding the fluorophore eYFP (AAV5/EF1a-fDIO-eYFP-WPRE; UNC, 3.8×10^{12}) bilaterally into the BLA at AP -1.6, ML ±3.3, DV -5.1. After at least 6 weeks, we performed a second surgery to label BLA neurons projecting to the medial prefrontal cortex (mPFC) through injection of a retrograde tracer (200 nL cholera toxin b subunit fused to Alexa-647, CTB-647) in the mPFC (AP 1.8, ML ±0.35, DV -2).

ex vivo Electrophysiology Recordings

One week after the CTB-647 surgery, mice were deeply anaesthetized via I.P. injection of sodium pentobarbital (200 mg/kg) prior to transcardial perfusion with 20 mL ice-cold modified artificial cerebrospinal fluid (ACSF; composition in mM: 75 sucrose, 87 NaCl, 25 $NaHCO_3$, 2.5 KCl, 1.3 $NaH_2PO_4*H_2O$, 7 $MgCl_2*6H_2O$, 0.5 $CaCl_2*2H_2O$, 5 ascorbic acid, in ddH_2O; osmolarity 324-328 mOsm, pH 7.3-7.4) saturated with carbogen gas (95% oxygen, 5% carbon dioxide). The brain was quickly dissected out of the cranial cavity and a semiautomatic vibrating blade microtome (VT1200; Leica, IL, USA) was then used to prepare 300 µm thick coronal slices containing the BLA. Brain slices encompassing the basal forebrain and mPFC were also collected for verification of ChR2-mCherry and CTB-647 expression, respectively. Slices were then transferred to ACSF (composition in mM: 126 NaCl, 2.5 KCl, 26 $NaHCO_3$, 1.25 $NaH_2PO_4*H_2O$, 1 $MgCl_2*6H_2O$, 2.4 $CaCl_2*2H_2O$, and 10 glucose, in ddH_2O; osmolarity 299-301 mOsm; pH 7.30-7.40) saturated with carbogen gas (95% oxygen, 5% carbon dioxide) in a water bath kept at 30-32 °C. They were allowed to recover for at least 1 h before transfer to the recording chamber for electrophysiological recordings.

In the recording chamber BLA slices were continually perfused with carbogen-saturated ACSF, at a temperature of 31±1 °C, via a peristaltic pump (Minipuls3; Gilson, WI, USA). BLA neurons were visualized through an upright microscope (Scientifica, UK) using infra-red differential interference contrast (IR-DIC) optics and a Q-imaging Retiga Exi camera (Q Imaging, Canada). Identification of eYFP+ GABAergic neurons and CTB-647-expressing mPFC-projector neurons was achieved through a 40X water-immersion objective using brief fluorescence illumination from a 470 nm LED light source (pE-100; CoolLED, NY, USA) or a metal halide lamp (Lumen 200, Prior Scientific Inc., MA, USA), respectively, through appropriate excitation/emission filters (Olympus, PA, USA). Thin walled borosilicate glass capillary tubing was shaped into microelectrodes for recording using a horizontal puller (P-97, Sutter Instruments, CA, USA) and had resistance values of 3-6 MΩ when filled with internal solution (composition in mM: 125 potassium gluconate, 20 HEPES, 10 NaCl, 3 MgATP, and 0.1% neurobiotin (pH 7.30-7.33; 286-287 mOsm). Recorded signals were amplified with a Multiclamp 700B amplifier (Molecular Devices, CA, USA), low-pass filtered at 3 kHz, digitized at 10 kHz using a Digidata 1550, and recorded using pClamp 10.4 software (Molecular Devices, CA, USA). Series resistance, input resistance, and holding current were monitored throughout experiments via a 5 mV, 0.1 sec step. Any significant changes were interpreted as signs of cell deterioration and recordings were terminated. To assess the response of BLA neurons to cholinergic input, ChR2-expressing cholinergic terminals were activated by trains of 5 ms pulses of 470 nm light (pE-100; CoolLED, NY, USA) delivered through the 40X objective every 30 s, while recording in current-clamp mode. To isolate monosynaptic currents tetrodotoxin (TTX; 1 µM; Tocris, MN, USA) and 4-Aminopyridine (4AP; 1 mM, Sigma, MO, USA) were included in the ACSF (Petreanu et al., 2007). Scopolamine (10 µM; Sigma, MO, USA) was used to block muscarinic ACh receptors, and a cocktail of nicotinic antagonists (dihydro-ß-erythroidine (10 µM, Tocris, MN, USA), methyllycaconitine (0.1 µM; Sigma, MO, USA), and mecamylamine (10 µM; Sigma, MO, USA)) was used to block nicotinic ACh receptors. Offline analysis of peak current amplitude was performed in Clampfit 10.4 (Molecular Devices, CA, USA). Capacitance and membrane resistance (Rm) were calculated from a 5 mV, 0.1 sec hyperpolarizing step in voltage-clamp using custom MATLAB software written by Praneeth Namburi based on MATLAB implementation of the Q-method (Novák and Zahradník, 2006).

ex vivo Electrophysiology Histology

Following recording, slices were fixed in 4% PFA overnight at 4 °C then washed in PBS (4x 10 min). To reveal neurobiotin-labelled cells, recorded slices were blocked in PBS containing 0.3% Triton (PBS-T 0.3%) and 3% normal donkey serum (NDS; Jackson ImmunoResearch, USA) at room temperature for 60 min before incubation in PBS-T 0.3% with 3% NDS and CF405-conjugated streptavidin (1:1000; Biotium, CA, USA). After 90 min slices were washed in PBS (4x 10 min) then mounted onto glass slides and coverslipped using polyvinyl alcohol mounting medium with DABCO (Sigma, MO, USA). Images of the BLA were captured using a confocal laser scanning microscope (Olympus FV1000), with FluoView software (Olympus, PA, USA). Neurobiotin-filled recorded neurons were imaged at high magnification through a 40X/1.3 NA oil-immersion objective using serial z-stacks with an optical slice thickness of 3 µm.

Immunohistochemistry

After behavioral experiments, mice were anaesthetized with pentobarbital sodium (200 mg/kg), and transcardially perfused with ice-cold Ringer's solution followed by ice-cold 4% PFA in PBS (pH 7.3). Brains were extracted and fixed in 4% PFA for 24 hours and equilibrated in 30% sucrose in PBS for 3 days. Coronal sections were cut at 40 µm using a sliding microtome (HM430; Thermo Fisher Scientific) and kept in PBS at 4°C until antibody staining.

Sections from the PFC, BF, and BLA were taken for immunohistochemistry. Sections were washed six times for five minutes each in 1x PBS, and then blocked for 2 hours at room temperature in 3% normal donkey serum in 0.3% PBS-Triton. Sections were then incubated overnight at room temperature in blocking solution with primary antibody goat-anti-ChAT (1:200 / 1:100) or chicken-anti-GFP (1:500). The next day, sections were washed six times for five minutes in 1x PBS. Sections were then incubated in secondary antibody donkey-anti-goat 488 or 555 (1:500) or donkey-anti-chicken 488 (1:1000) in blocking solution at room temperature for 2 hours. Finally, sections were washed six times for five minutes in 1x PBS and mounted on microscope slides using a Vectashield mounting medium with DAPI. Slides were sealed with clear nail polish to preserve sections. All washing and staining steps were done covered on a shaker.

Confocal Microscopy Fluorescent images were captured using a confocal laser scanning microscope (Olympus FV1000), with FluoView software (Olympus, PA, USA), under a 10X / 0.40 NA dry objective or a 40X /1.30 NA oil immersion objective. Images were subsequently processed in Adobe Illustrator (Adobe Systems Incorporated, CA, USA). Similar to prior work, we also observed some ectopic expression of ChAT (Hedrick et al., 2016), particularly in later litters of breeding pairs, and excluded these mice based on postmortem histological examination.

Acknowledgments

We thank C. Wildes, R. Wichmann, J. Wang, A. Heynen for technical assistance. We thank V. Breton-Provencher, J. Shih, M. Sur, and the members of the Bear lab for additional support. We thank A. Sutton, M. Picciotto, R. Crouse, A. Kepecs, F. Sturgill, and E. Calipari for helpful discussions.

The authors declare no competing interests.

Funding: E.Y.K. was supported by NIH grant K08-MH116135 (NIMH). C.A.S. was supported by an NIH grant R00 DA04510 (NIDA), a NARSAD Young Investigator Award (Brain and Behavior Research Foundation), and by an Alkermes Pathways Research Award grant, an independent competitive grants program supported by Alkermes. M.F. was supported by NIH grant K99-EY029326 (National Eye Institute). D.B.P. was supported by R01-DC017078 and funding from the Nancy Lurie Marks Family Foundation. K.M.T. is an HHMI investigator and the Wylie Vale chair at Salk Institute for Biological Studies, a New York Stem Cell Foundation - Robertson Investigator and McKnight Scholar and this work was supported by funding from the JPB Foundation, the PIIF, PNDRF, JFDP, Alfred P Sloan Foundation, New York Stem Cell Foundation, Klingenstein Foundation, McKnight Foundation, Clayton Foundation, Dolby Family Fund, R01-MH102441 (NIMH), R01-MH115920 (NIMH), RF1-AG047661 (NIA), the NIH Director's New Innovator Award DP2-DK102256 (NIDDK), and Pioneer Award DP1-AT009925 (NCCIH).

Author Contributions

Conceptualization, E.Y.K. and K.M.T.;

Methodology, E.Y.K., A.B-R., G.A.M., C.A.S., M.J., Y.L., and K.M.T.;

Software, E.Y.K.;

Validation, E.Y.K., T.C., and M.P.;

Formal Analysis, E.Y.K.;

Investigation, E.Y.K., A.B-R., G.A.M., T.C., M.P., J.W., W.Y., S.F., R.S., and M.F.;

Resources, Y.K., D.B.P., and K.M.T.;

Writing – Original Draft, E.Y.K., A.B-R., G.A.M., T.C., M.P., C.A.S., and K.M.T.;

Writing – Review & Editing, D.B.P.;

Funding Acquisition, E.Y.K, D.B.P., and K.M.T.;

References

Adelsberger H, Garaschuk O, Konnerth A. 2005. Cortical calcium waves in resting newborn mice. *Nat Neurosci* **8**:988–990. doi:10.1038/nn1502

Adermark L, Söderpalm B, Burkhardt JM. 2014. Brain region specific modulation of ethanol-induced depression of GABAergic neurons in the brain reward system by the nicotine receptor antagonist mecamylamine. *Alcohol Fayettev N* **48**:455–461. doi:10.1016/j.alcohol.2014.06.004

Aitta-Aho T, Hay YA, Phillips BU, Saksida LM, Bussey TJ, Paulsen O, Apergis-Schoute J. 2018. Basal Forebrain and Brainstem Cholinergic Neurons Differentially Impact Amygdala Circuits and Learning-Related Behavior. *Curr Biol CB* **28**:2557-2569.e4. doi:10.1016/j.cub.2018.06.064

Allaway KC, Muñoz W, Tremblay R, Sherer M, Herron J, Rudy B, Machold R, Fishell G. 2020. Cellular birthdate predicts laminar and regional cholinergic projection topography in the forebrain. *eLife* **9**:e63249. doi:10.7554/eLife.63249

American Psychiatric Association. 2013. Diagnostic and Statistical Manual of Mental Disorders, 5th Edition: DSM-5, 5 edition. ed. Washington, D.C: American Psychiatric Publishing.

Bakin JS, Weinberger NM. 1996. Induction of a physiological memory in the cerebral cortex by stimulation of the nucleus basalis. *Proc Natl Acad Sci U S A* **93**:11219–11224. doi:10.1073/pnas.93.20.11219

Ballinger EC, Ananth M, Talmage DA, Role LW. 2016. Basal Forebrain Cholinergic Circuits and Signaling in Cognition and Cognitive Decline. *Neuron* **91**:1199–1218. doi:10.1016/j.neuron.2016.09.006

Bates D, Mächler M, Bolker B, Walker S. 2015. Fitting Linear Mixed-Effects Models Using lme4. *J Stat Softw* **67**:1–48. doi:10.18637/jss.v067.i01

Baxter MG, Chiba AA. 1999. Cognitive functions of the basal forebrain. *Curr Opin Neurobiol* **9**:178–183. doi:10.1016/s0959-4388(99)80024-5

Beninger RJ, Dringenberg HC, Boegman RJ, Jhamandas K. 2001. Cognitive effects of neurotoxic lesions of the nucleus basalis magnocellularis in rats: differential roles for corticopetal versus amygdalopetal projections. *Neurotox Res* **3**:7–21. doi:10.1007/BF03033227

Biederman J, Mick E, Faraone S, Hammerness P, Surman C, Harpold T, Dougherty M, Aleardi M, Spencer T. 2006. A double-blind comparison of galantamine hydrogen bromide and placebo in adults with attention-deficit/hyperactivity disorder: a pilot study. *J Clin Psychopharmacol* **26**:163–166. doi:10.1097/01.jcp.0000204139.20417.8a

Bloem B, Schoppink L, Rotaru DC, Faiz A, Hendriks P, Mansvelder HD, Berg WDJ van de, Wouterlood FG. 2014. Topographic Mapping between Basal Forebrain Cholinergic Neurons and the Medial Prefrontal Cortex in Mice. *J Neurosci* **34**:16234–16246. doi:10.1523/JNEUROSCI.3011-14.2014

Boegman RJ, Cockhill J, Jhamandas K, Beninger RJ. 1992. Excitotoxic lesions of rat basal forebrain: differential effects on choline acetyltransferase in the cortex and amygdala. *Neuroscience* **51**:129–135. doi:10.1016/0306-4522(92)90477-j

Brown DA. 2019. Acetylcholine and cholinergic receptors. *Brain Neurosci Adv* **3**:2398212818820506. doi:10.1177/2398212818820506

Burgos-Robles A, Kimchi EY, Izadmehr EM, Porzenheim MJ, Ramos-Guasp WA, Nieh EH, Felix-Ortiz AC, Namburi P, Leppla CA, Presbrey KN, Anandalingam KK, Pagan-Rivera PA, Anahtar M, Beyeler A, Tye KM. 2017. Amygdala inputs to prefrontal cortex guide behavior amid conflicting cues of reward and punishment. *Nat Neurosci* **20**:824–835. doi:10.1038/nn.4553

Cardinal RN, Parkinson JA, Hall J, Everitt BJ. 2002. Emotion and motivation: the role of the amygdala, ventral striatum, and prefrontal cortex. *Neurosci Biobehav Rev* **26**:321–352. doi:10.1016/s0149-7634(02)00007-6

Carlsen J, Záborszky L, Heimer L. 1985. Cholinergic projections from the basal forebrain to the basolateral amygdaloid complex: a combined retrograde fluorescent and immunohistochemical study. *J Comp Neurol* **234**:155–167. doi:10.1002/cne.902340203

Chen E, Lallai V, Sherafat Y, Grimes NP, Pushkin AN, Fowler JP, Fowler CD. 2018. Altered Baseline and Nicotine-Mediated Behavioral and Cholinergic Profiles in ChAT-Cre Mouse Lines. *J Neurosci* 1433–17. doi:10.1523/JNEUROSCI.1433-17.2018

Chen T-W, Wardill TJ, Sun Y, Pulver SR, Renninger SL, Baohan A, Schreiter ER, Kerr RA, Orger MB, Jayaraman V, Looger LL, Svoboda K, Kim DS. 2013. Ultrasensitive fluorescent proteins for imaging neuronal activity. *Nature* **499**:295–300. doi:10.1038/nature12354

Chintoh A, Fulton J, Koziel N, Aziz M, Sud M, Yeomans JS. 2003. Role of cholinergic receptors in locomotion induced by scopolamine and oxotremorine-M. *Pharmacol Biochem Behav* **76**:53–61. doi:10.1016/s0091-3057(03)00196-5

Chubykin AA, Roach EB, Bear MF, Shuler MGH. 2013. A cholinergic mechanism for reward timing within primary visual cortex. *Neuron* **77**:723–735. doi:10.1016/j.neuron.2012.12.039

Crouse RB, Kim K, Batchelor HM, Girardi EM, Kamaletdinova R, Chan J, Rajebhosale P, Pittenger ST, Role LW, Talmage DA, Jing M, Li Y, Gao X-B, Mineur YS, Picciotto MR. 2020. Acetylcholine is released in the basolateral amygdala in response to predictors of reward and enhances the learning of cue-reward contingency. *eLife* **9**:e57335. doi:10.7554/eLife.57335

Cubo E, Fernández Jaén A, Moreno C, Anaya B, González M, Kompoliti K. 2008. Donepezil use in children and adolescents with tics and attention-deficit/hyperactivity disorder: an 18-week, single-center, dose-escalating, prospective, open-label study. *Clin Ther* **30**:182–189. doi:10.1016/j.clinthera.2008.01.010

Cui G, Jun SB, Jin X, Pham MD, Vogel SS, Lovinger DM, Costa RM. 2013. Concurrent activation of striatal direct and indirect pathways during action initiation. *Nature* **494**:238–242. doi:10.1038/nature11846

Dasgupta R, Seibt F, Beierlein M. 2018. Synaptic Release of Acetylcholine Rapidly Suppresses Cortical Activity by Recruiting Muscarinic Receptors in Layer 4. *J Neurosci Off J Soc Neurosci* **38**:5338–5350. doi:10.1523/JNEUROSCI.0566-18.2018

Ferguson JE, Boldt C, Redish AD. 2009. Creating low-impedance tetrodes by electroplating with additives. *Sens Actuators Phys* **156**:388–393. doi:10.1016/j.sna.2009.10.001

Ferster CB, Skinner BF. 1957. Variable IntervalSchedules of Reinforcement, Century Psychology Series. New York: Appleton-Century-Crofts. pp. 355–364.

Franklin KBJ. 2008. The mouse brain in stereotaxic coordinates, 3rd ed. ed. Amsterdam; Boston: Elsevier/Academic Press.

Gielow MR, Zaborszky L. 2017. The Input-Output Relationship of the Cholinergic Basal Forebrain. *Cell Rep* **18**:1817–1830. doi:10.1016/j.celrep.2017.01.060

Gritton HJ, Howe WM, Mallory CS, Hetrick VL, Berke JD, Sarter M. 2016. Cortical cholinergic signaling controls the detection of cues. *Proc Natl Acad Sci U S A* **113**:E1089-1097. doi:10.1073/pnas.1516134113

Gunaydin LA, Grosenick L, Finkelstein JC, Kauvar IV, Fenno LE, Adhikari A, Lammel S, Mirzabekov JJ, Airan RD, Zalocusky KA, Tye KM, Anikeeva P, Malenka RC, Deisseroth K. 2014. Natural neural projection dynamics underlying social behavior. *Cell* **157**:1535–1551. doi:10.1016/j.cell.2014.05.017

Guo W, Robert B, Polley DB. 2019. The Cholinergic Basal Forebrain Links Auditory Stimuli with Delayed Reinforcement to Support Learning. *Neuron* **103**:1164-1177.e6. doi:10.1016/j.neuron.2019.06.024

Hangya B, Ranade SP, Lorenc M, Kepecs A. 2015. Central Cholinergic Neurons Are Rapidly Recruited by Reinforcement Feedback. *Cell* **162**:1155–1168. doi:10.1016/j.cell.2015.07.057

Harrison TC, Pinto L, Brock JR, Dan Y. 2016. Calcium Imaging of Basal Forebrain Activity during Innate and Learned Behaviors. *Front Neural Circuits* **10**:36. doi:10.3389/fncir.2016.00036

Hasselmo ME, Sarter M. 2011. Modes and Models of Forebrain Cholinergic Neuromodulation of Cognition. *Neuropsychopharmacology* **36**:52. doi:10.1038/npp.2010.104

He K, Zhang X, Ren S, Sun J. 2016. Deep Residual Learning for Image Recognition2016 IEEE Conference on Computer Vision and Pattern Recognition (CVPR). Presented at the 2016 IEEE Conference on Computer Vision and Pattern Recognition (CVPR). pp. 770–778. doi:10.1109/CVPR.2016.90

Heckers S, Mesulam M-M. 1994. Two types of cholinergic projections to the rat amygdala. *Neuroscience* **60**:383–397. doi:10.1016/0306-4522(94)90252-6

Heckers S, Ohtake T, Wiley RG, Lappi DA, Geula C, Mesulam MM. 1994. Complete and selective cholinergic denervation of rat neocortex and hippocampus but not amygdala by an immunotoxin against the p75 NGF receptor. *J Neurosci Off J Soc Neurosci* **14**:1271–1289.

Hedrick T, Danskin B, Larsen RS, Ollerenshaw D, Groblewski P, Valley M, Olsen S, Waters J. 2016. Characterization of Channelrhodopsin and Archaerhodopsin in Cholinergic Neurons of Cre-Lox Transgenic Mice. *PloS One* **11**:e0156596. doi:10.1371/journal.pone.0156596

Herman AM, Ortiz-Guzman J, Kochukov M, Herman I, Quast KB, Patel JM, Tepe B, Carlson JC, Ung K, Selever J, Tong Q, Arenkiel BR. 2016. A cholinergic basal forebrain feeding circuit modulates appetite suppression. *Nature* **538**:253–256. doi:10.1038/nature19789

Higley MJ, Picciotto MR. 2014. Neuromodulation by Acetylcholine: Examples from Schizophrenia and Depression. *Curr Opin Neurobiol* **0**:88–95. doi:10.1016/j.conb.2014.06.004

Hshieh TT, Fong TG, Marcantonio ER, Inouye SK. 2008. Cholinergic deficiency hypothesis in delirium: a synthesis of current evidence. *J Gerontol A Biol Sci Med Sci* **63**:764–772.

Insafutdinov E, Pishchulin L, Andres B, Andriluka M, Schiele B. 2016. DeeperCut: A Deeper, Stronger, and Faster Multi-person Pose Estimation Model In: Leibe B, Matas J, Sebe N, Welling M, editors. Computer Vision – ECCV 2016, Lecture Notes in Computer Science. Cham: Springer International Publishing. pp. 34–50. doi:10.1007/978-3-319-46466-4_3

Jiang L, Kundu S, Lederman JD, López-Hernández GY, Ballinger EC, Wang S, Talmage DA, Role LW. 2016. Cholinergic Signaling Controls Conditioned Fear Behaviors and Enhances Plasticity of Cortical-Amygdala Circuits. *Neuron* **90**:1057–1070. doi:10.1016/j.neuron.2016.04.028

Jing M, Li Yuexuan, Zeng J, Huang P, Skirzewski M, Kljakic O, Peng W, Qian T, Tan K, Zou J, Trinh S, Wu R, Zhang S, Pan S, Hires SA, Xu M, Li H, Saksida LM, Prado VF, Bussey TJ, Prado MAM, Chen L, Cheng H, Li Yulong. 2020. An optimized acetylcholine sensor for monitoring in vivo cholinergic activity. *Nat Methods* **17**:1139–1146. doi:10.1038/s41592-020-0953-2

Jing M, Zhang P, Wang G, Feng J, Mesik L, Zeng J, Jiang H, Wang S, Looby JC, Guagliardo NA, Langma LW, Lu J, Zuo Y, Talmage DA, Role LW, Barrett PQ, Zhang LI, Luo M, Song Y, Zhu JJ, Li Y. 2018. A genetically encoded fluorescent acetylcholine indicator for in vitro and in vivo studies. *Nat Biotechnol* **36**:726–737. doi:10.1038/nbt.4184

Kalmbach A, Hedrick T, Waters J. 2012. Selective optogenetic stimulation of cholinergic axons in neocortex. *J Neurophysiol* **107**:2008–2019. doi:10.1152/jn.00870.2011

Kim CK, Yang SJ, Pichamoorthy N, Young NP, Kauvar I, Jennings JH, Lerner TN, Berndt A, Lee SY, Ramakrishnan C, Davidson TJ, Inoue M, Bito H, Deisseroth K. 2016. Simultaneous fast measurement of circuit dynamics at multiple sites across the mammalian brain. *Nat Methods* **13**:325–328. doi:10.1038/nmeth.3770

Kitt CA, Höhmann C, Coyle JT, Price DL. 1994. Cholinergic innervation of mouse forebrain structures. *J Comp Neurol* **341**:117–129. doi:10.1002/cne.903410110

Kruk M, Tendera K, Biała G. 2011. Memory-related effects of cholinergic receptor ligands in mice as measured by the elevated plus maze test. *Pharmacol Rep PR* **63**:1372–1382. doi:10.1016/s1734-1140(11)70701-0

Kruk-Słomka M, Michalak A, Budzyńska B, Biała G. 2014. A comparison of mecamylamine and bupropion effects on memory-related responses induced by nicotine and scopolamine in the novel object recognition test in mice. *Pharmacol Rep PR* **66**:638–646. doi:10.1016/j.pharep.2014.02.002

Kuznetsova A, Brockhoff PB, Christensen RHB. 2017. lmerTest Package: Tests in Linear Mixed Effects Models. *J Stat Softw* **82**:1–26. doi:10.18637/jss.v082.i13

Laszlovszky T, Schlingloff D, Hegedüs P, Freund TF, Gulyás A, Kepecs A, Hangya B. 2020. Distinct synchronization, cortical coupling and behavioral function of two basal forebrain cholinergic neuron types. *Nat Neurosci*. doi:10.1038/s41593-020-0648-0

Lee S, Kim J-H. 2019. Basal Forebrain Cholinergic-induced Activation of Cholecystokinin Inhibitory Neurons in the Basolateral Amygdala. *Exp Neurobiol* **28**:320–328. doi:10.5607/en.2019.28.3.320

Lenth RV. 2020. emmeans.

Letzkus JJ, Wolff SBE, Meyer EMM, Tovote P, Courtin J, Herry C, Lüthi A. 2011. A disinhibitory microcircuit for associative fear learning in the auditory cortex. *Nature* **480**:331–335. doi:10.1038/nature10674

Li X, Yu B, Sun Q, Zhang Y, Ren M, Zhang X, Li A, Yuan J, Madisen L, Luo Q, Zeng H, Gong H, Qiu Z. 2018. Generation of a whole-brain atlas for the cholinergic system and mesoscopic projectome analysis of basal forebrain cholinergic neurons. *Proc Natl Acad Sci U S A* **115**:415–420. doi:10.1073/pnas.1703601115

Likhtik E, Johansen JP. 2019. Neuromodulation in circuits of aversive emotional learning. *Nat Neurosci* **22**:1586–1597. doi:10.1038/s41593-019-0503-3

Likhtik E, Pelletier JG, Paz R, Paré D. 2005. Prefrontal control of the amygdala. *J Neurosci Off J Soc Neurosci* **25**:7429–7437. doi:10.1523/JNEUROSCI.2314-05.2005

Likhtik E, Stujenske JM, Topiwala MA, Harris AZ, Gordon JA. 2014. Prefrontal entrainment of amygdala activity signals safety in learned fear and innate anxiety. *Nat Neurosci* **17**:106–113. doi:10.1038/nn.3582

Liu C-H, Coleman JE, Davoudi H, Zhang K, Hussain Shuler MG. 2015. Selective activation of a putative reinforcement signal conditions cued interval timing in primary visual cortex. *Curr Biol CB* **25**:1551–1561. doi:10.1016/j.cub.2015.04.028

Lutas A, Fernando K, Zhang SX, Sambangi A, Andermann ML. 2022. History-dependent dopamine release increases cAMP levels in most basal amygdala glutamatergic neurons to control learning. *Cell Rep* **38**:110297. doi:10.1016/j.celrep.2022.110297

Lutas A, Kucukdereli H, Alturkistani O, Carty C, Sugden AU, Fernando K, Diaz V, Flores-Maldonado V, Andermann ML. 2019. State-specific gating of salient cues by midbrain dopaminergic input to basal amygdala. *Nat Neurosci* **22**:1820–1833. doi:10.1038/s41593-019-0506-0

Lütcke H, Murayama M, Hahn T, Margolis DJ, Astori S, Zum Alten Borgloh SM, Göbel W, Yang Y, Tang W, Kügler S, Sprengel R, Nagai T, Miyawaki A, Larkum ME, Helmchen F, Hasan MT. 2010. Optical recording of neuronal activity with a genetically-encoded calcium indicator in anesthetized and freely moving mice. *Front Neural Circuits* **4**:9. doi:10.3389/fncir.2010.00009

Mathis A, Mamidanna P, Cury KM, Abe T, Murthy VN, Mathis MW, Bethge M. 2018. DeepLabCut: markerless pose estimation of user-defined body parts with deep learning. *Nat Neurosci* **21**:1281–1289. doi:10.1038/s41593-018-0209-y

Matthews GA, Nieh EH, Vander Weele CM, Halbert SA, Pradhan RV, Yosafat AS, Glober GF, Izadmehr EM, Thomas RE, Lacy GD, Wildes CP, Ungless MA, Tye KM. 2016. Dorsal Raphe Dopamine

Neurons Represent the Experience of Social Isolation. *Cell* **164**:617–631. doi:10.1016/j.cell.2015.12.040

McDonald AJ, Mascagni F. 2011. Neuronal localization of M2 muscarinic receptor immunoreactivity in the rat amygdala. *Neuroscience* **196**:49–65. doi:10.1016/j.neuroscience.2011.08.032

McDonald AJ, Mascagni F. 2010. Neuronal localization of m1 muscarinic receptor immunoreactivity in the rat basolateral amygdala. *Brain Struct Funct* **215**:37–48. doi:10.1007/s00429-010-0272-y

McDonald AJ, Muller JF, Mascagni F. 2011. Postsynaptic targets of GABAergic basal forebrain projections to the basolateral amygdala. *Neuroscience* **183**:144–159. doi:10.1016/j.neuroscience.2011.03.027

McGaughy J, Dalley JW, Morrison CH, Everitt BJ, Robbins TW. 2002. Selective behavioral and neurochemical effects of cholinergic lesions produced by intrabasalis infusions of 192 IgG-saporin on attentional performance in a five-choice serial reaction time task. *J Neurosci Off J Soc Neurosci* **22**:1905–1913.

Morandi A, Lucchi E, Turco R, Morghen S, Guerini F, Santi R, Gentile S, Meagher D, Voyer P, Fick D, Schmitt EM, Inouye SK, Trabucchi M, Bellelli G. 2015a. Delirium superimposed on dementia: A quantitative and qualitative evaluation of patient experience. *J Psychosom Res* **79**:281–287. doi:10.1016/j.jpsychores.2015.07.010

Morandi A, Lucchi E, Turco R, Morghen S, Guerini F, Santi R, Gentile S, Meagher D, Voyer P, Fick DM, Schmitt EM, Inouye SK, Trabucchi M, Bellelli G. 2015b. Delirium superimposed on dementia: A quantitative and qualitative evaluation of informal caregivers and health care staff experience. *J Psychosom Res* **79**:272–280. doi:10.1016/j.jpsychores.2015.06.012

Muller JF, Mascagni F, Zaric V, Mott DD, McDonald AJ. 2016. Localization of the M2 muscarinic cholinergic receptor in dendrites, cholinergic terminals, and noncholinergic terminals in the rat basolateral amygdala: An ultrastructural analysis. *J Comp Neurol* **524**:2400–2417. doi:10.1002/cne.23959

Nath T, Mathis A, Chen AC, Patel A, Bethge M, Mathis MW. 2019. Using DeepLabCut for 3D markerless pose estimation across species and behaviors. *Nat Protoc* **14**:2152–2176. doi:10.1038/s41596-019-0176-0

Nelson A, Mooney R. 2016. The Basal Forebrain and Motor Cortex Provide Convergent yet Distinct Movement-Related Inputs to the Auditory Cortex. *Neuron* **90**:635–648. doi:10.1016/j.neuron.2016.03.031

Newman EL, Gupta K, Climer JR, Monaghan CK, Hasselmo ME. 2012. Cholinergic modulation of cognitive processing: insights drawn from computational models. *Front Behav Neurosci* **6**:24. doi:10.3389/fnbeh.2012.00024

Nieh EH, Matthews GA, Allsop SA, Presbrey KN, Leppla CA, Wichmann R, Neve R, Wildes CP, Tye KM. 2015. Decoding Neural Circuits that Control Compulsive Sucrose Seeking. *Cell* **160**:528–541. doi:10.1016/j.cell.2015.01.003

Nieh EH, Vander Weele CM, Matthews GA, Presbrey KN, Wichmann R, Leppla CA, Izadmehr EM, Tye KM. 2016. Inhibitory Input from the Lateral Hypothalamus to the Ventral Tegmental Area Disinhibits Dopamine Neurons and Promotes Behavioral Activation. *Neuron* **90**:1286–1298. doi:10.1016/j.neuron.2016.04.035

Novák P, Zahradník I. 2006. Q-method for high-resolution, whole-cell patch-clamp impedance measurements using square wave stimulation. *Ann Biomed Eng* **34**:1201–1212. doi:10.1007/s10439-006-9140-6

O'Malley G, Leonard M, Meagher D, O'Keeffe ST. 2008. The delirium experience: A review. *J Psychosom Res* **65**:223–228. doi:10.1016/j.jpsychores.2008.05.017

Parikh V, Kozak R, Martinez V, Sarter M. 2007. Prefrontal acetylcholine release controls cue detection on multiple timescales. *Neuron* **56**:141–154. doi:10.1016/j.neuron.2007.08.025

Peck CJ, Salzman CD. 2014. The amygdala and basal forebrain as a pathway for motivationally guided attention. *J Neurosci Off J Soc Neurosci* **34**:13757–13767. doi:10.1523/JNEUROSCI.2106-14.2014

Petreanu L, Huber D, Sobczyk A, Svoboda K. 2007. Channelrhodopsin-2-assisted circuit mapping of long-range callosal projections. *Nat Neurosci* **10**:663–668. doi:10.1038/nn1891

Pidoplichko VI, Prager EM, Aroniadou-Anderjaska V, Braga MFM. 2013. α7-Containing nicotinic acetylcholine receptors on interneurons of the basolateral amygdala and their role in the regulation of the network excitability. *J Neurophysiol* **110**:2358–2369. doi:10.1152/jn.01030.2012

Pinto L, Goard MJ, Estandian D, Xu M, Kwan AC, Lee S-H, Harrison TC, Feng G, Dan Y. 2013. Fast modulation of visual perception by basal forebrain cholinergic neurons. *Nat Neurosci* **16**:1857–1863. doi:10.1038/nn.3552

Potter AS, Schaubhut G, Shipman M. 2014. Targeting the nicotinic cholinergic system to treat attention-deficit/hyperactivity disorder: rationale and progress to date. *CNS Drugs* **28**:1103–1113. doi:10.1007/s40263-014-0208-9

Prado MAM, Reis RAM, Prado VF, de Mello MC, Gomez MV, de Mello FG. 2002. Regulation of acetylcholine synthesis and storage. *Neurochem Int* **41**:291–299. doi:10.1016/s0197-0186(02)00044-x

R Core Team. 2015. R: A Language and Environment for Statistical Computing.

Robert B, Kimchi EY, Watanabe Y, Chakoma T, Jing M, Li Y, Polley DB. 2021. A functional topography within the cholinergic basal forebrain for encoding sensory cues and behavioral reinforcement outcomes. *eLife* **10**:e69514. doi:10.7554/eLife.69514

Rossi J, Balthasar N, Olson D, Scott M, Berglund E, Lee CE, Choi MJ, Lauzon D, Lowell BB, Elmquist JK. 2011. Melanocortin-4 receptors expressed by cholinergic neurons regulate energy balance and glucose homeostasis. *Cell Metab* **13**:195–204. doi:10.1016/j.cmet.2011.01.010

Równiak M, Kolenkiewicz M, Kozłowska A. 2017. Parvalbumin, but not calretinin, neurons express high levels of α1-containing GABAA receptors, α7-containing nicotinic acetylcholine receptors and D2-dopamine receptors in the basolateral amygdala of the rat. *J Chem Neuroanat* **86**:41–51. doi:10.1016/j.jchemneu.2017.08.002

Rye DB, Wainer BH, Mesulam MM, Mufson EJ, Saper CB. 1984. Cortical projections arising from the basal forebrain: a study of cholinergic and noncholinergic components employing combined retrograde tracing and immunohistochemical localization of choline acetyltransferase. *Neuroscience* **13**:627–643. doi:10.1016/0306-4522(84)90083-6

Siddiqi N, Harrison JK, Clegg A, Teale EA, Young J, Taylor J, Simpkins SA. 2016. Interventions for preventing delirium in hospitalised non-ICU patients. *Cochrane Database Syst Rev* **3**:CD005563. doi:10.1002/14651858.CD005563.pub3

Singh J, Kour K, Jayaram MB. 2012. Acetylcholinesterase inhibitors for schizophrenia. *Cochrane Database Syst Rev* **1**:CD007967. doi:10.1002/14651858.CD007967.pub2

Sturgill JF, Hegedus P, Li SJ, Chevy Q, Siebels A, Jing M, Li Y, Hangya B, Kepecs A. 2020. Basal forebrain-derived acetylcholine encodes valence-free reinforcement prediction error. *bioRxiv* 2020.02.17.953141. doi:10.1101/2020.02.17.953141

Thany SH, Tricoire-Leignel H. 2011. Emerging Pharmacological Properties of Cholinergic Synaptic Transmission: Comparison between Mammalian and Insect Synaptic and Extrasynaptic Nicotinic Receptors. *Curr Neuropharmacol* **9**:706–714. doi:10.2174/157015911798376343

Thiele A, Bellgrove MA. 2018. Neuromodulation of Attention. *Neuron* **97**:769–785. doi:10.1016/j.neuron.2018.01.008

Tye KM, Tye LD, Cone JJ, Hekkelman EF, Janak PH, Bonci A. 2010. Methylphenidate facilitates learning-induced amygdala plasticity. *Nat Neurosci* **13**:475–481.

Unal CT, Pare D, Zaborszky L. 2015. Impact of basal forebrain cholinergic inputs on basolateral amygdala neurons. *J Neurosci Off J Soc Neurosci* **35**:853–863. doi:10.1523/JNEUROSCI.2706-14.2015

Vander Weele CM, Siciliano CA, Matthews GA, Namburi P, Izadmehr EM, Espinel IC, Nieh EH, Schut EHS, Padilla-Coreano N, Burgos-Robles A, Chang C-J, Kimchi EY, Beyeler A, Wichmann R, Wildes CP, Tye KM. 2018. Dopamine enhances signal-to-noise ratio in cortical-brainstem encoding of aversive stimuli. *Nature* **563**:397–401. doi:10.1038/s41586-018-0682-1

Venkatesan S, Jeoung H-S, Chen T, Power SK, Liu Y, Lambe EK. 2020. Endogenous Acetylcholine and Its Modulation of Cortical Microcircuits to Enhance Cognition. *Curr Top Behav Neurosci* **45**:47–69. doi:10.1007/7854_2020_138

Washburn MS, Moises HC. 1992. Muscarinic responses of rat basolateral amygdaloid neurons recorded in vitro. *J Physiol* **449**:121–154.

Woodruff AR, Sah P. 2007. Networks of parvalbumin-positive interneurons in the basolateral amygdala. *J Neurosci Off J Soc Neurosci* **27**:553–563. doi:10.1523/JNEUROSCI.3686-06.2007

Woolf NJ, Eckenstein F, Butcher LL. 1984. Cholinergic systems in the rat brain: I. projections to the limbic telencephalon. *Brain Res Bull* **13**:751–784.

Zaborszky L, Pol AN van den, Gyengesi E. 2012. The Basal Forebrain Cholinergic Projection System in Mice. *Mouse Nerv Syst* 684–718. doi:10.1016/B978-0-12-369497-3.10028-7

Zachariou V, Caldarone BJ, Weathers-Lowin A, George TP, Elsworth JD, Roth RH, Changeux JP, Picciotto MR. 2001. Nicotine receptor inactivation decreases sensitivity to cocaine. *Neuropsychopharmacol Off Publ Am Coll Neuropsychopharmacol* **24**:576–589. doi:10.1016/S0893-133X(00)00224-4

Zhu PJ, Stewart RR, McIntosh JM, Weight FF. 2005. Activation of nicotinic acetylcholine receptors increases the frequency of spontaneous GABAergic IPSCs in rat basolateral amygdala neurons. *J Neurophysiol* **94**:3081–3091. doi:10.1152/jn.00974.2004

Figure Legends

Figure 1 Photostimulation of basal forebrain cholinergic neurons promotes conditioned responding when associated with the opportunity to collect rewards

(A) Window of Opportunity Task (WoOT) to study conditioned responding in the absence of discrete cues. Mice were trained prior to any photostimulation, using an operant, variable-interval reinforcement schedule with limited hold (Ferster and Skinner, 1957). Sessions were divided into trials of 3-second *Windows of Opportunity*, with variable intertrial intervals (ITIs). Rewards were only delivered if mice licked during an unsignaled *Window of Opportunity* (green; 90% of trial windows). We also included a subset of *Unrewarded Windows*, on which, even if the mouse licked, reward would not be delivered (purple; 10% of trial windows), similar to intervening ITIs (white). Because windows were not discretely cued and occurred after variable ITIs, mice did not know when they initiated a lick whether it would be rewarded.

(B) Sample WoOT behavior. If a mouse licked during an uncued *Windows of Opportunity* (green), then reward was delivered. But if a mouse licked during an uncued *Unrewarded Window* (purple) or during the ITI (white), reward was not delivered. reward delivery. The use of *Unrewarded Windows* (purple) allowed us to investigate behavior during epochs temporally matched to *Windows of Opportunity* (green). Training mice in this manner conditioned them to lick the spout with a relatively stable pattern of intermittent lick bouts (Figure S1).

(C) Optogenetic strategy to photostimulate cholinergic basal forebrain neurons, by driving Cre-dependent expression of Channelrhodopsin-2 (ChR2) or a control fluorophore (eYFP) in mice expressing Cre-recombinase under control of the choline acetyltransferase promoter (ChAT::Cre). The photostimulation parameters displayed were used in later behavioral sessions.

(D) Sample histology of fiber placement over cholinergic neurons in the posterior portion of the basal forebrain, the sublenticular substantia innominata/extended amygdala. Blue=DAPI nucleic acid staining, Green=cre-dependent expression of ChR2 fused to eYFP, Red=anti-ChAT immunohistochemical staining. AP coordinate = -0.46. Scale bar = 500 microns. See also Figure S1A-B.

(E) Behavioral training and testing sessions. After early WoOT training without any photostimulation, mice subsequently received testing during a Photostim-Unreinforced or Photostim-Reinforced sessions.

(F) Photostim-Unreinforced Session. In addition to no photostimulation *Windows of Opportunity* (green, 80%) and *Unrewarded Windows* (purple, 8%), mice received 2 sec of photostimulation (blue lines) during a subset of *Unrewarded Windows* (purple, 12%) to study innate responses to photostimulation.

(G) Photostim-Reinforced Session. Conversely to Photostim-Unreinforced sessions, during Photostim-Reinforced sessions, photostimulation (blue lines) was delivered during a subset of *Windows of Opportunity* (green, 12%), during which, if mice licked, they would receive a reward. Mice still had many more *Windows of Opportunity* with no photostimulation (68%).

(H & I) The likelihood of licking depended on an interaction of Virus, Photostimulation Window type, and Photostim-Reinforcement Session type (linear mixed effects model, $F_{1,78}$=5.26, p=0.025). Thin lines represent data from all individual mice, pooled data are represented as mean ± SEM. During the Photostim-Unreinforced Session (H), there was no significant difference between ChR2 (blue) and eYFP (gray) groups, regardless of photostimulation window type. However, during the Photostim-Reinforced Session (I), ChR2 mice licked significantly more during Photostim windows than No Photostim windows (post-hoc tests with Sidak correction for multiple comparisons: ***p<0.0001). ChR2 mice also licked significantly more than eYFP mice during Photostim windows during Photostim-Reinforced sessions (**p=0.001). There were no detectable effects of photostimulation on licking in eYFP mice, and no detectable differences in licking on no photostimulation windows between ChR2 and eYFP mice (all other post-hoc comparisons p>0.10).

(J) We initially photostimulated with a fixed duration, but in a follow-up session photostimulated with varied durations (0-0.5 sec, using different number of pulses at the same frequency/duty cycle). The likelihood of licking depended on an interaction of Virus and the number of photostimulation pulses (linear mixed effects model, $F_{3,84}$=16.22, p=2.1x10^{-8}). ChR2 mice licked significantly more on windows with 1, 2, or 10 pulses than windows without photostimulation, and more than eYFP mice with any number of pulses (post-hoc tests with Sidak correction for multiple comparisons: *p=0.015, **p=0.0095, ***p<0.001; all other post-hoc comparisons p>0.10).

(K) When tested with different durations of photostimulation, the latency of the first lick depended on an interaction of Virus and the number of photostimulation pulses (linear mixed effects model, $F_{3,84}$=4.53, p=0.005). ChR2 mice licked significantly sooner on windows with 1, 2, or 10 pulses than windows without photostimulation, and sooner than eYFP mice for 2 and 10 pulses (post-hoc tests with Sidak correction for multiple comparisons: **p=0.0047, ***p<0.001; all other post-hoc comparisons p>0.10).

Figure 2 BF^{ChAT}:ChR2-induced conditioned responding is muscarinic receptor-dependent

(A) Experimental strategy to test the necessity of cholinergic receptors in conditioned responding. Cholinergic neurons in the basal forebrain were photostimulated after blockade of cholinergic muscarinic or nicotinic receptors using intraperitoneal injection of pharmacologic antagonists.

(B) Modification of Window of Opportunity Task (WoOT) to include additional tone conditioned responses. To provide additional within-subject controls for pharmacologic testing, mice could now receive rewards on either of two separate types of *Windows of Opportunity*: with tones (top row) or with photostimulation (middle row, both 2 sec duration). Licks during unsignaled, *Unrewarded Windows* were recorded but had no consequence (bottom row).

(C) Photostim-induced licking was abolished by systemic muscarinic receptor antagonist administration. Linear mixed effects modelling confirmed that licking depended upon an interaction between Virus group, Stimulus type, and Drug session ($F_{3,363}$=4.61, p=0.0002). Thin lines represent data from individual mice, pooled data are displayed as mean ± SEM. Saline: Both ChR2 and eYFP mice responded more during Tone *Windows of Opportunity* than during unsignaled, *Unrewarded Windows* (Unrwd) (***p<0.001, *p<0.05, #p=0.10, Sidak post-hoc multiple comparisons). However, only ChR2 mice responded more during Photostimulation *Windows of Opportunity* than during unsignaled, *Unrewarded Windows*, at a similar likelihood as their responses during tone *Windows of Opportunity*. Scopolamine 0.3mg/kg: ChR2 mice now responded less during photostimulation than during tones. Scopolamine 1mg/kg: ChR2 mice no longer responded more during photostimulation than during *Unrewarded Windows*, and no longer responded more during photostimulation than eYFP mice, although they continued to respond more during tones than ITIs. Mecamylamine 1mg/kg: Response patterns were similar to Saline sessions. For each session, the likelihood of licking during *Unrewarded Windows* was similar between ChR2 and eYFP mice (all p>0.8). Additionally, within each group, the likelihood of licking during *Unrewarded Windows* was similar to Saline sessions for all drug doses (all p>0.8).

Figure 3 Cholinergic basal forebrain neural activity increases during conditioned stimuli and responses, even in the absence of reward delivery

(A) Strategy to record fluorescent activity from basal forebrain cholinergic neurons expressing the calcium sensor GCaMP6s, using interleaved signal (470 nm, blue) and reference (405 nm, violet) wavelengths to elicit fluorescence (525 nm, green).

(B) Task windows. We recorded fluorescent activity from mice during a traditional operant cue detection task. If mice licked after the onset of a tone, a fluid reward was delivered after a 0.5 sec delay. Licks during the silent *Unrewarded Windows* had no consequence.

(C) Sample GCaMP photometry fluorescence traces from one mouse demonstrating signal increases around the times of tones, licks, and reward deliveries. Increases were apparently present even for licking in the absence of tones and rewards. The blue trace represents data from the signal wavelength (470 nm) and the violet trace represents interleaved data from the reference wavelength (405 nm).

(D) Changes in fluorescence from basal forebrain cholinergic neurons referenced to the time of tone onset. Heat maps represent trial-averaged data from each mouse. Top heat maps are for 470 nm excited fluorescence (Signal 470), bottom heat maps are for 405 nm reference (Ref 405). The bottom panel summary data are represented as mean ± SEM. Mice are sorted in all heat maps (D-F, I-J), in the order of average post-lick activity in panel E.

(E) Changes in fluorescence from basal forebrain cholinergic neurons referenced to the time of the first lick after tone onset. Licking triggered subsequent reward delivery (first lick at 0 sec, reward delivery at dashed line, 0.5 sec).

(F) Changes in fluorescence from basal forebrain cholinergic neurons referenced to the onset of matched lick bouts that were in the absence of tone cues and did not lead to reward delivery.

(G) Fluorescence levels from basal forebrain cholinergic neurons at baseline (-2 to -1.5 sec before each referenced event) and post-event time points (0 to 0.5 sec after events, to standardize analyses between events) in the Cued task. Fluorescence levels depended on an interaction of Wavelength, Time point, and Event type (linear mixed effects model, $F_{2,55}$=3.28, p=0.045). Fluorescence levels increased at the time of events in the 470 nm wavelength signal channel (blue), but not the 405 reference channel (violet) (Tone: t_{55}=2.64, #p=0.064; Lick leading to Reward Delivery (Lick & Rwd): t_{55}=7.57, ***p<0.001; Licks in absence of Cue & Reward Delivery (Lick, No Rwd): t_{55}=5.29, ***p<0.001; Sidak correction for six multiple comparisons). Thin lines represent data from all individual mice, pooled data are represented as mean ± SEM.

(H) Uncued Window of Opportunity Task (WoOT). All mice were also recorded from at an earlier stage of WoOT training, before experience with tones or other discrete cues. If a mouse licked during an uncued *Window of Opportunity*, a fluid reward was delivered. A 0.5 sec delay was instituted between lick and reward to account for the slow dynamics of GCaMP6s. Licks during *Unrewarded Windows* were recorded but had no consequence.

(I) Changes in fluorescence from basal forebrain cholinergic neurons referenced to the time of the first lick that triggered reward delivery (first lick at 0 sec, reward delivery at dashed line, 0.5 sec).

(J) Changes in fluorescence from basal forebrain cholinergic neurons referenced to the onset of matched lick bouts that did not lead to reward delivery.

(K) Fluorescence levels from basal forebrain cholinergic neurons at baseline (-2 to -1.5 sec before each referenced event) and post-event time points (0 to 0.5 sec after events, to standardize analyses between events) in WoOT. Fluorescence levels depended on an interaction of Wavelength and Time point (linear mixed effects model, $F_{1,35}$=13.59, p=0.0008), without a third order interaction by Event type ($F_{1,35}$=0.02, p=0.882). Fluorescence levels increased at the time of events in the 470 nm wavelength signal channel (blue), but not the 405 reference channel (violet) (Lick leading to Reward Delivery (Lick & Rwd): t_{35}=3.58, **p=0.004; Licks in absence of Reward Delivery (Lick, No Rwd): t_{35}=3.90, **p<0.002; Sidak correction for four multiple comparisons). Thin lines represent data from all individual mice, pooled data are represented as mean ± SEM.

Figure 4 Local ACh levels in the BLA, measured using a genetically-encoded sensor, increase during conditioned stimuli and responses

(A) Strategy to record local ACh levels in the BLA. A genetically-encoded, fluorescent ACh sensor (GACh3.0, (B)) was expressed in BLA neurons, and imaged using interleaved signal (470 nm, blue) and reference (405 nm, violet) wavelengths to elicit fluorescence (525 nm, green).

(B) The fluorescent ACh sensor, GACh3.0, is a fusion protein between a modified M3 muscarinic receptor and cyclically permuted GFP. GACh3.0 undergoes a conformational change and fluoresces to 470nm light after binding ACh. Please note that kinetics for GACh3.0(Jing et al., 2020) are somewhat faster than those for GCaMP6s.(Chen et al., 2013)

(C) Cued task windows. We recorded fluorescent activity from mice during a traditional operant cue detection task. If mice licked after the onset of a tone, a fluid reward was delivered after a 0.1 sec delay. Licks during ITIs had no consequence.

(D) Sample BLA ACh sensor fluorescence traces from one mouse demonstrating apparent increases around the times of tones, licks, and reward deliveries. Increases were apparently present even for licking in the absence of tones and rewards.

(E) Changes in BLA ACh sensor fluorescence referenced to the time of tone onset. Heat maps represent trial-averaged data from each mouse. Top heat maps are for 470 nm excited fluorescence (Signal 470), bottom heat maps are for 405 nm reference (Ref 405). The bottom panel summary data are represented as mean ± SEM. Mice are sorted in all heat maps (E-G, J-K), in the order of average post-lick activity in panel F.

(F) Changes in BLA ACh sensor fluorescence referenced to the time of the first lick after tone onset. Licking triggered reward delivery (first lick at 0 sec, reward delivery at dashed line, 0.5 sec).

(G) Changes in BLA ACh sensor fluorescence referenced to the onset of matched lick bouts that were in the absence of tone cues and did not lead to reward delivery.

(H) BLA ACh sensor fluorescence levels at baseline (-2 to -1.5 sec before each referenced event) and post-event time points (0 to 0.5 sec after events, to standardize analyses between events) in the Cued task. Fluorescence levels depended on an interaction of Wavelength and Time point (linear mixed effects model, $F_{1,99}$=20.41, p<0.001), without a third order interaction by Event type ($F_{2,99}$=1.20, p=0.305). Fluorescence levels increased at the time of events in the 470 nm wavelength signal channel (blue), but not the 405 reference channel (violet) (Tone: t_{99}=2.80, *p=0.036; Lick leading to Reward Delivery (Lick & Rwd): t_{99}=5.49, ***p<0.001; Licks in absence of Cue & Reward Delivery (Lick, No Rwd): t_{99}=2.91, *p<0.027; Sidak correction for six multiple comparisons). Thin lines represent data from all individual mice, pooled data are represented as mean ± SEM.

(I) Uncued Window of Opportunity Task (WoOT). All mice were also recorded from at an earlier stage of WoOT training, before experience with tones or other discrete cues. If a mouse licked during an uncued *Window of Opportunity*, a fluid reward was delivered. Licks during *Unrewarded Windows* were recorded but had no consequence.

(J) Changes in BLA ACh sensor fluorescence referenced to the time of the first lick that triggered reward delivery (first lick at 0 sec, reward delivery at dashed line, 0.1 sec).

(K) Changes in BLA ACh sensor fluorescence referenced to the onset of matched lick bouts that did not lead to reward delivery.

(L) BLA ACh sensor fluorescence levels at baseline (-2 to -1.5 sec before each referenced event) and post-event time points (0 to 0.5 sec after events, to standardize analyses between events) in WoOT. Fluorescence levels depended on an interaction of Wavelength and Time point (linear mixed effects model, $F_{1,63}$=44.21, $p<0.001$), without a third order interaction by Event type ($F_{1,63}$=1.25, $p=0.267$). Fluorescence levels increased at the time of events in the 470 nm wavelength signal channel (blue), but not the 405 reference channel (violet) (Lick leading to Reward Delivery (Lick & Rwd): t_{63}=8.41, ***$p<0.001$; Licks in absence of Reward Delivery (Lick, No Rwd): t_{63}=5.94, ***$p<0.001$; Sidak correction for four multiple comparisons). Thin lines represent data from all individual mice, pooled data are represented as mean ± SEM.

Figure 5 Cholinergic signaling in the BLA is sufficient to promote conditioning responding but ACh release is independent of reward contingency

(A) Optogenetic strategy to photostimulate cholinergic (ChAT::Cre) basal forebrain terminals in the BLA selectively.

(B) The difference in the likelihood of licking between Photostim and No Photostim windows differed depending on the window in which photostimulation was delivered. The effect of photostimulation within each session is calculated for each mouse. A linear mixed-effects model to account for repeated measures demonstrated that the effect of photostimulation depended on an interaction between Virus and Session type ($F_{1,15}$ = 9.624, p = 0.007). Post-hoc tests Sidak correction for multiple comparisons revealed that the effect of photostimulation was greater for ChR2 mice in Photostim-Reinforced than Photostim-Unreinforced sessions (***p=0.0004), and that the effect of photostimulation in Photostim-Reinforced sessions was greater for ChR2 mice than eYFP mice (*p=0.0215). All other comparisons were not significant (p>0.05).

(C) Schematic showing concurrent photostimulation of cholinergic terminals in the BLA while measuring local ACh using a genetically-encoded fluorescent sensor, through the same optic fiber. Mice either expressed ChrimsonR or a control fluorophore (tdTomato) in basal forebrain ChAT neurons.

(D) Sample fluorescent traces from ACh sensor (orange) from a mouse with ChrimsonR, in relationship to reward delivery (red), licks (black), behavioral windows (Reward green/Unrewarded purple), and photostimulation (orange). Photostimulation was either delivered in a Photostim-Unreinforced session (during *Unrewarded Windows*, left, purple) or Photostim-Reinforced session (during rewarded windows, right, green).

(E) Sample ACh fluorescent traces from ACh sensor (gray) from a mouse with a control fluorophore, displayed similarly to (E), in relationship to rewards, licks, behavioral windows, and photostimulation, delivered either in a Photostim-Unreinforced (left, purple) or Photostim-Reinforced session (right, green).

(F) Heat maps comparing average ACh measurements for each mouse around the time of photostimulation on the Photostim-Unreinforced session. Mice are separated based on whether they expressed ChrimsonR (orange, n=6) or control fluorophore (gray, n=4). Summary data in the bottom panel are represented as mean ± SEM. Mice are sorted in all panels based mean DF/F during laser stimulation.

(G) Heat maps comparing average ACh measurements for each mouse during photostimulation in the Photostim-Reinforced session. Conventions are as in (G), and mice are sorted in the same order as in (G).

(H) Mean ACh measurements evoked by photostimulation on the Unreinforced (left) or Reinforced (right) session. Evoked ACh measurements were higher for ChrimsonR mice than control fluorophore mice, but evoked ACh measurements did not depend upon whether photostimulation was provided on Unreinforced or Reinforced sessions (linear mixed effects model: effect of Virus $F_{1,8}$=20.21, **p=0.002; effect of Session $F_{1,8}$=0.47, p=0.51; interaction between Virus and Session type $F_{1,8}$=0.86, p=0.38).

Figure 6 Cholinergic modulation of neural activity *in vivo* depends upon reward context in the amygdala, but not in the prefrontal cortex

(A) Strategy for photostimulation of cholinergic basal forebrain neurons and terminal region electrophysiology in the dorsomedial prefrontal cortex (dmPFC) and basolateral amygdala (BLA). Six ChR2 mice had electrodes implanted in both dmPFC and BLA. Five ChR2 mice had electrodes implanted only in the BLA, yielding a total of 11 ChR2 mice with electrodes in BLA. Photostimulation parameters were the same as in ChR2 behavioral experiments (Fig 1).

(B) Activity from all recorded neurons in each target area (dmPFC and BLA, total 963 neurons over all sessions from 11 mice), from sessions in which photostimulation was delivered during ITI *Unrewarded Windows* (Photostim-Unreinforced, purple) or sessions in which photostimulation was delivered during *Windows of Opportunity* (Photostim-Reinforced, green). Each row represents activity from a single neuron, normalized to baseline (-2 to 0 sec before photostimulation onset), and smoothed with a 50 ms Gaussian. Neurons are sorted according to mean activity during photostimulation (0 to +2 sec). Summary population data in the bottom panels are represented as mean ± SEM. Black marks underneath the population data represent 10 ms steps when the population activity differed between Photostim-Unreinforced vs. Photostim-Reinforced sessions (rank-sum test, $p<0.01$).

(C) Licking activity from all mice contributing recordings for each target area, from sessions in which photostimulation was delivered during ITI *Unrewarded Windows* (Photostim-Unreinforced, purple) or sessions in which photostimulation was delivered during *Windows of Opportunity* (Photostim-Reinforced, green). Each row represents activity from a single mouse. Summary population data in the bottom panels are represented as mean ± SEM. Black marks underneath the population data represent 10 ms steps when the population licking activity differed between Photostim-Unreinforced vs. Photostim-Reinforced sessions (rank-sum test, $p<0.01$).

(D) Example neural activity from each target area (dmPFC left, BLA right) around photostimulation of basal forebrain cholinergic neurons (0-2 sec), from Photostim-Unreinforced sessions. Top panels are individual trial rasters and black markers indicate the first lick following Photostim onset. Trials are sorted by lick latency. Summary data in the bottom panels are represented as mean ± SEM, smoothed with a 50 ms Gaussian kernel. We observed neurons that were facilitated and suppressed relative to baseline in both regions (signed-rank test of firing rate in the 1 sec before stimulation vs 0.5 sec after, $p<0.01$).

(E) Example neural activity from each target area (dmPFC left, BLA right) around photostimulation of basal forebrain cholinergic neurons (0-2 sec), from Photostim-Reinforced sessions. We again observed neurons that were facilitated and suppressed relative to baseline in both regions. Conventions are the same as in (E).

(F) Proportions of neurons that were facilitated (solid bars) or suppressed (open bars) in each area during Photostim-Unreinforced sessions (purple) or Photostim-Reinforced sessions (green). Denominator n's refer to neurons recorded across all mice during each session type. A higher percentage of BLA neurons were suppressed on Photostim-Reinforced sessions than Photostim-Unreinforced sessions (2-sample tests for equality of proportions: $X^2=6.81$, df=1,

*p=0.036, corrected for 4 multiple comparisons using Holm's procedure). There was a trend towards a lower percentage of BLA neurons being facilitated on Photostim-Reinforced sessions than Photostim-Unreinforced sessions (X^2=4.52, df=1, #p=0.10).

(G) Proportions of neurons that were facilitated (solid bars) or suppressed (open bars) in each area during Photostim-Unreinforced sessions (left, purple) or Photostim-Reinforced sessions (right, green). Data is replotted from (E) to facilitate comparisons between areas for each session type. A higher percentage of BLA neurons than dmPFC neurons were suppressed during both Photostim-Unreinforced and Photostim-Reinforced sessions (2-sample tests for equality of proportions: Photostim-Unreinforced: X^2=13.11, df=1, ***p<0.001; Photostim-Reinforced: X^2=35.61, df=1, ***p<0.001; all p values corrected for 4 multiple comparisons using Holm's procedure). A lower percentage of BLA neurons than PFC neurons were facilitated during Photostim-Reinforced sessions (X^2=9.21, df=1, **p=0.005).

Figure 7 Cholinergic afferents suppress basolateral amygdala output through muscarinic receptors and feed-forward inhibition

(A) Schematic of injection strategy to express ChR2 in cholinergic neurons of the basal forebrain (BF) and eYFP in GABAergic neurons of the BLA (BLA^{GABA}), using conditional viral expression in ChAT::Cre x VGAT::Flpo mice (VGAT = vesicular GABAergic transporter), along with CTB-647 as a retrograde marker of neurons projecting to dmPFC.

(B) Confocal image of the BLA showing whole-cell patch-clamp recording arrangement in the BLA with optical stimulation of ChR2-expressing BF terminals. AP coordinate = -1.58.

(C) High magnification images of neurobiotin-filled recorded BLA neurons expressing CTB-647 (BLA-mPFC; upper panels) and eYFP (BLA^{GABA}, lower panels).

(D) Passive membrane properties of BLA-mPFC and BLA^{GABA} neurons. BLA-mPFC neurons had significantly greater capacitance (unpaired t-test: t_{42}=11.90, ***p<0.001, n=20 BLA-mPFC, n=24 BLA^{GABA}, from 9 mice), smaller membrane resistance (unpaired t-test: t_{42}=6.326, ***p<0.001, n=20 BLA-mPFC, n=24 BLA^{GABA} , from 9 mice), and more negative resting membrane potential (unpaired t-test: t_{29}=2.857, **p=0.0078, n=13 BLA-mPFC, n=18 BLA^{GABA} , from 8 mice) than BLA^{GABA} neurons.

(E) Example trace and frequency histogram showing suppression of firing in BLA-mPFC neurons and facilitation of firing of BLA^{GABA} neurons following optical stimulation of cholinergic terminals (470 nm light, 20 Hz; scale bars=20 mV, 5 s).

(F) Membrane potential of BLA-mPFC (upper traces) and BLA^{GABA} neurons (lower traces) in response to 1 s 470 nm light delivered at 5, 10, and 20 Hz in current-clamp.

(G) At each stimulation frequency the amplitude of the fast excitatory postsynaptic potential (EPSP) was greater in BLA^{GABA} neurons (green) compared with BLA-mPFC neurons (magenta; 2-way ANOVA, main effect of cell type: $F_{1,40}$=95.59, ***p<0.001; n=7, 7, 15 BLA-mPFC neurons at 5, 10, 20 Hz, n=5, 5, 7 BLA^{GABA} neurons at 5, 10, 20 Hz, from 9 mice), while the slower inhibitory postsynaptic current (IPSP) was greater in BLA-mPFC neurons (2-way ANOVA, main effect of cell type: $F_{1,40}$=47.29, ***p<0.001; n=7, 7, 15 BLA-mPFC neurons at 5, 10, 20 Hz, n=5, 5, 7 BLA^{GABA} neurons at 5, 10, 20 Hz, from 9 mice).

(H) Response of BLA-mPFC (upper traces) and BLA^{GABA} neurons (lower traces) to a single 5 ms pulse of 470 nm light, with application of TTX/4AP to isolate monosynaptic currents.

(I) Following application of TTX/4AP, the EPSP was maintained in BLA^{GABA} neurons (green; unpaired t-test: t_{15}=0.367, p=0.719, n=8 (ACSF) and n=9 (TTX/4AP) BLA^{GABA} cells from 4 mice), while the IPSP was maintained in BLA-mPFC neurons (magenta; unpaired t-test: t_{16}=0.094, p=0.926, n=9 (ACSF) and n=9 (TTX/4AP) BLA-mPFC cells from 3 mice).

(J) Example traces showing inhibition of the IPSP in BLA-mPFC neurons (upper panels) by the muscarinic receptor antagonist scopolamine (10 µM) (dark gray), but not nicotinic antagonists (dihydro-ß-erythroidine 10 µM, methyllycaconitine 0.1 µM, mecamylamine 10 µM) (light gray), and inhibition of the EPSP in BLA^{GABA} neurons (lower panels) by nicotinic receptor antagonists, but not muscarinic.

(K) Proposed circuit model showing BF inhibition of BLA output by ACh acting at nicotinic receptors on BLA^{GABA} neurons and muscarinic receptors on projection neurons. Dashed lines represent local BLA^{GABA} neuron synapses onto BLA projector neurons from prior literature (Lee and Kim, 2019; Woodruff and Sah, 2007).

Figure S1 Training history was similar for optogenetic experimental ChR2 mice and control eYFP mice

(A) Histological evaluation of basal forebrain tissue. Blue=DAPI nucleic acid staining, Green=cre-dependent expression of ChR2-eYFP, Red=anti-ChAT immunohistochemical staining. Yellow overlap indicates ChAT+ cells expressing ChR2-eYFP.

(B) Validation of ChR2 expression in ChAT::Cre neurons. 88.9% of ChR2 expressing cells were also immunoreactive for ChAT (442/497 cells, 18 total sections from 3 mice).

(C) After surgery, mice were trained on the Window of Opportunity Task (WoOT) prior to any photostimulation, until they attempted to collect rewards on at least 30% of uncued *Windows of Opportunity*. The number of training sessions to reach this criterion were similar for ChR2 and eYFP mice (ChR2: n=17 mice, 7.53 ± 1.22 sessions; eYFP: n=11 mice, 7.00 ± 1.61 sessions; rank-sum p=0.49). Pooled data are represented as mean (horizontal lines) ± SEM (vertical lines) in this and all subsequent panels, all of which represent training after surgery but prior to any photostimulation.

(D) On the WoOT training session on which mice met criterion prior to any photostimulation, ChR2 and eYFP mice were similarly likely to lick on unsignaled *Windows of Opportunity* as on *Unrewarded Windows*, confirming that mice could not predict reward delivery prior to licking (Figure 1C; linear mixed effects model: effect of Virus p=0.859, effect of *Window of Opportunity* type p=0.744, interaction between Virus*Window p=0.652).

(E) The number of rewards earned in a session were similar between both groups of mice (ChR2: 292.47 ± 29.08 rewards; eYFP: 269.45 ± 23.85 rewards; rank-sum p=0.71).

(F) Session mean licking rates were similar between both groups of mice (ChR2: 1.08 ± 0.14 licks/sec; eYFP: 1.19 ± 0.22 licks/sec; rank-sum p=0.81).

(G) The majority of licks occurred within bouts, defined as at least 3 licks with inter-lick intervals of ≤0.3sec. The percentages of licks in bouts were similar between both groups of mice (ChR2: 79 ± 3%; eYFP: 77 ± 4%; rank-sum p=0.96).

(H) The median numbers of licks in a bout were similar between both groups of mice (ChR2: 4.94 ± 0.26 licks/bout; eYFP: 5.27 ± 0.49 licks/bout; rank-sum p=0.73).

(I) The median intervals between bouts were similar between both groups of mice (ChR2: 7.75 ± 1.16 sec; eYFP: 8.87 ± 1.91 sec; rank-sum p=0.78).

Figure S2 Responses across the WoOT photostimulation testing sessions

(A) The likelihood of licking depended on an interaction of Virus, Photostimulation Window type, and Session (linear mixed effects model, $F_{2,130}$=3.34, p=0.038). Thin lines represent data from all individual mice, pooled data are represented as mean ± SEM. During the Photostim-Unreinforced Session, there was no significant difference between ChR2 (blue) and eYFP (gray) mice, regardless of photostimulation window type. However, during the Photostim-Reinforced Sessions, ChR2 mice started to lick more during Photostim windows than No Photostim windows. ChR2 mice also began to trend to lick more over sessions during Photostim windows than eYFP mice (post-hoc tests with Sidak correction for multiple comparisons: #p<0.10, *p<0.05, **p<0.01, ***p<0.001). There were no detectable effects of photostimulation on licking in eYFP mice, and no detectable differences in licking on No Photostim windows between ChR2 and eYFP mice (all other post-hoc comparisons p>0.10).

(B) Lick latencies depended on an interaction of Virus and Photostimulation Window (linear mixed effects model, $F_{1,128}$=15.20, p=0.0002). During the Photostim-Unreinforced Session, there was no significant difference between ChR2 (blue) and eYFP (gray) mice, regardless of photostimulation window type. However, during the Photostim-Reinforced Sessions, ChR2 mice licked with significantly shorter latencies during Photostim windows than No Photostim windows. ChR2 mice also licked with significantly shorter latencies than eYFP mice during Photostim windows (post-hoc tests with Sidak correction for multiple comparisons: *p<0.05, **p<0.01, ***p<0.001). There were no detectable effects of photostimulation on lick latencies in eYFP mice, and no detectable differences in lick latencies on No Photostim windows between ChR2 and eYFP mice (all other post-hoc comparisons p>0.10).

(C) Photostimulation on a ***previous*** trial did not affect the likelihood of licking in a subsequent window. In this panel, trials are split based on whether animals received photostimulation on the ***previous*** trial. There was no significant interaction between Virus, ***Previous*** photostimulation, and Session (linear mixed effects model, (linear mixed effects model, $F_{2,130}$=0.33, p=0.717).

(D) An additional Photostim-Unreinforced session did not lead to increased licking during photostimulation windows (n=6 ChR2 mice). There were no significant main effects of Photostimulation Window (linear mixed effects model, $F_{1,15}$=0.431, p=0.521), Session ($F_{1,15}$=0.359, p=0.558), or an interaction between them ($F_{1,15}$=0.009, p=0.926).

(E) An additional Photostim-Unreinforced (P-U2) session after Photostim-Reinforced (P-R 1&2) training led to decreased licking during photostimulation windows (n=3 ChR2 mice). In all 3 mice, response rates from the Photostim-Reinforced 2 (P-R2) session decreased during a subsequent Photostim-Unreinforced session (P-U2, paired t-test p=0.005), suggesting that the association between photostimulation and reinforcement remained plastic.

Figure S3 Peri-event licking across the WoOT photostimulation testing sessions

(A) Detailed licking profiles of two individual ChR2 mice along all three sessions of the WoOT photostimulation assay process. For photostimulation trials, the laser was turned on from 0 to 2 sec. Summary plots depict mean ± SEM for all panels.

(B) Detailed licking profiles of two individual eYFP mice along all three sessions of the WoOT photostimulation assay process.

(C) For all mice mouse across all sessions, licking is presented synchronized to the times of WoOT windows (Peri-Window). Each row depicts stratified results by viral group, and colors depict whether trials involved photostimulation.

(D) For each mouse for each session, licking is presented synchronized to reward onset (Peri-Reward), stratified by viral group (row) and whether the trial involved photostimulation (color). There were not any photostimulation trials around the time of reward for the Photostim-Unreinforced sessions, since photostimulation was only delivered when reward could not be obtained. Across subsequent sessions, there was no clear effect of photostimulation on licking or reward consumption behavior in either ChR2 (n=17) or eYFP (n=11) mice.

Figure S4 Photostimulation of basal forebrain cholinergic neurons increases arousal, but does not increase unconditioned movement and is not inherently reinforcing

(A) Optogenetic strategy for photostimulation of basal forebrain cholinergic (ChAT::Cre) neurons. The same photostimulation parameters (473 nm, 4mW, 5 ms pulses at 20 Hz) were used for all ChR2 and eYFP experiments.

(B) Open field test protocol. Mice explored an open chamber for three contiguous windows, during which photostimulation was off for 5 min, then on for 5 min, then off again for the last 5 min. Example tracks are shown for a ChR2 mouse (dark blue, top row) and an eYFP mouse (gray, bottom row).

(C) Basal forebrain cholinergic photostimulation did not increase mouse locomotor movement in an open field (linear mixed effects model: effect of Time $F_{1,15}$=19.18, ***p<0.0001; effect of Virus $F_{1,7.26}$=0.71, p=0.43; effect of Photostim $F_{1,15}$=0.20, p=0.66; interaction between Virus and Photostim $F_{1,15}$=0.33, p=0.58).

(D) Photostimulation of cholinergic basal forebrain neurons did not modify innate locomotor preference, as measured by time spent in the center of the open field (linear mixed effects model: effect of Time $F_{1,15}$=2.90, p=0.11; effect of Virus $F_{1,7.39}$=0.01, p=0.94; effect of Photostim $F_{1,15}$=1.64, p=0.22; interaction between Virus and Photostim $F_{1,15}$=0.04, p=0.85).

(E) Real-time place preference (RTPP) assay. When mice entered the Laser On zone, photostimulation was activated for the duration of the time spent in the On zone. When mice entered the Laser Off zone, photostimulation was terminated for the duration of time spent in the Off zone.

(F) Neither ChR2 nor eYFP mice preferred the chamber side paired with photostimulation (averaged results of two counterbalanced sessions for each mouse, t-test ChR2 t_{16}=0.94, p=0.36; eYFP t_7=0.08, p=0.94), suggesting that photostimulation of cholinergic basal forebrain neurons was not inherently reinforcing.

(G) We trained a subset of mice to perform the Window of Opportunity Task (WoOT) while on a treadmill to measure unconditioned, spontaneous locomotion during photostimulation. Heat maps: Mean velocity for each mouse on photostimulation trials in 10 ms bins. Data are stratified by Virus group and sorted by mean velocity during the Photostim-Unreinforced session. Bottom panels: Pooled data are displayed as mean ± SEM. There was no significant difference in locomotion around photostimulation between the ChR2 and eYFP groups during either the Photostim-Unreinforced or Photostim-Reinforced sessions (no 10 ms bins were significantly different between groups on either day, rank-sum p<0.05, uncorrected).

(H) Mean velocity on the treadmill during photostimulation (0-2 sec) for Photostim-Unreinforced (left) and Photostim-Reinforced (right) sessions did not differ between groups or by sessions (linear mixed effects model: Virus*Session $F_{1,20}$=0.09, p=0.769; effect of Virus $F_{1,37}$=0.02, p=0.887; effect of Session $F_{1,20}$=1.26, p=0.275).

(I) We measured pupil diameter in a subset of mice as an index of arousal. Heat maps: Mean change in pupil diameter across laser trials for each mouse for the Photostim-Unreinforced session (left), and Photostim-Reinforced session (right). Data are normalized to

baseline pupil diameter -2 to -1 sec before photostimulation, and sorted by mean pupil diameter during the Unreinforced session. Bottom panels: Pooled data are displayed as mean ± SEM (ChR2: blue, n=16; eYFP: gray, n=10). Black marks underneath pooled data signify frames (33.3 ms bins) during which pupil responses were different between ChR2 and eYFP (rank-sum $p<0.05$, uncorrected).

(J) Mean change in pupil diameter after photostimulation onset (0-4 sec), for Photostim-Unreinforced (left) and Photostim-Reinforced (right) sessions. Mean pupil change depended on Viral Group and Session Type (linear mixed effects model: Virus*Session $F_{1,24}=4.37$, *$p=0.047$; effect of Virus $F_{1,24}=24.40$, ***$p<0.001$; effect of Session $F_{1,24}=2.01$, $p=0.169$). ChR2 mice had greater pupil dilation during the Photostim-Reinforced session than during their Photostim-Unreinforced session (post-hoc tests with Sidak correction for multiple comparisons: *$p<0.05$). ChR2 mice also had greater pupil dilation than eYFP mice during the Photostim-Reinforced session (***$p<0.001$). During the Photostim-Unreinforced session, there was a trend towards a small increase in pupil dilation in ChR2 mice vs eYFP mice (#$p=0.075$).

(K) Pupil diameter surrounding reward onset, during Photostim-Unreinforced (left) and Photostim-Reinforced (right) sessions, similar conventions as in (I), sorted in the same order as G. There was no significant difference between ChR2 and eYFP groups for any 10 ms bin (rank-sum $p<0.05$, uncorrected).

(L) Mean change in pupil diameter after reward onset (0-4sec), for Photostim-Unreinforced session (left) vs. Photostim-Reinforced sessions (right). Mean pupil change was independent of Viral Group and Session (linear mixed effects model: Virus*Session $F_{1,24}=2.43$, $p=0.132$; effect of Virus $F_{1,24}=0.01$, $p=0.942$; effect of Session $F_{1,24}=0.01$, $p=0.910$). Mean pupil change across all mice was greater than 0 (Linear mixed effects model: intercept 2.78%, $t_{24}=7.067$, ***$p<0.001$).

Figure S5 Comparison of ACh evoked by reward collection with that evoked by photostimulation

(A) Schematic showing strategy for concurrent photostimulation of cholinergic terminals in the BLA while measuring local ACh using a genetically-encoded fluorescent sensor, through the same optic fiber. Mice either expressed ChrimsonR or a control fluorophore (tdTomato) in basal forebrain ChAT neurons.

(B) Heat maps comparing average ACh measurements for each mouse around the time of reward delivery (left panel), or at the times of photostimulation of increasing duration (subsequent panels). Mice are separated based on whether they expressed ChrimsonR (orange, n=5) or control fluorophore (gray, n=4). Summary data in the bottom panels are represented as mean ± SEM. Mice are sorted in all panels based on the peri-reward activity in the first panel.

(C) Area Under the Curve (AUC) for %DF/F elicited by Reward (leftmost point) or increasing durations of photostimulation (1, 2, or 10 pulses), for mice with ChrimsonR (orange) or control fluorophore (gray). Data was analyzed for 0-0.5 sec after the event, consistent with the longest duration of photostimulation. Fluorescence levels depended upon an interaction between photostimulation duration and virus type (linear mixed effects model, $F_{3,21}$=10.36, p<0.001). Post-hoc tests compared to rewards showed that fluorescence changes only were greater for 10 pulses (t_{21}=5.24, ***p<0.001), and were most clearly greater in ChrimsonR mice than control fluorophore mice for increasing pulses (2 pulses $t_{16.5}$=2.98, #p=0.083; 10 pulses $t_{16.5}$=5.36, ***p<0.001; Sidak correction for ten comparisons). Summary data are represented as mean ± SEM.

Figure S6 Example neural variability and relationship to behavioral responses

Pairs of neurons recorded simultaneously from the dmPFC (left column) and BLA (middle column) during a Photostim-Unreinforced Session (top row) and Photostim-Reinforced Session (bottom row). Top panels indicate trial by trial rasters sorted by the first lick occurring in the window (orange circle), with bottom panels indicating average activity (smoothed with 100-ms Gaussian window). Rasters are split by whether they occurred during windows with photostimulation (purple or green), or matched windows without photostimulation.

Figure S7 Responses of neurons in the dmPFC and BLA to shorter photostimulations

(A) Strategy for photostimulation of cholinergic basal forebrain neurons and terminal region electrophysiology in the dorsomedial prefrontal cortex (dmPFC) and basolateral amygdala (BLA) with varying photostimulation durations. Three ChR2 mice had electrodes implanted in both dmPFC and BLA. Photostimulation parameters were the same as in ChR2 behavioral experiments (Fig 1).

(B) Activity from all recorded neurons in each target area (dmPFC and BLA, from 3 mice), from a session in which photostimulation was delivered during Rewarded windows at different durations (No photostimulation, 1 pulse, 2 pulses, or 10 pulses). Each row represents activity from a single neuron, normalized to baseline (-2 to 0 sec before photostimulation onset), and smoothed with a 50 ms Gaussian. Neurons are sorted according to mean activity after photostimulation (0 to +2 sec to maintain the same timing as prior figures) and represented under each trial type. Summary population data in the bottom panels for each photostimulation duration are represented as mean ± SEM. Green shaded marks underneath the population data represent 10 ms steps when the population activity differed between each duration of photostimulation and no photostimulation (sign-rank test, $p<0.01$).

(C) Licking activity from all mice contributing recordings to this figure. Each row represents activity from a single mouse for different photostimulation durations. Summary population data in the bottom panels are represented as mean ± SEM. The two plots are identical since the same mice were used for recordings in both areas, but are presented in duplicate to facilitate comparison with the plots above.

Figure S8 Effects of laser illumination on neural activity were not seen in control eYFP subjects

(A) Control strategy for laser illumination of cholinergic basal forebrain neurons expressing non-optogenetic fluorophore (eYFP). Four mice expressing eYFP in basal forebrain cholinergic neurons had electrodes implanted in both dmPFC and BLA. One eYFP mouse had electrodes implanted only in the BLA, yielding a total of five eYFP mice with electrodes in BLA.

(B) Activity from all recorded neurons in each area (total 449 neurons over two sessions per 5 control eYFP mice), from sessions in which laser illumination was delivered during ITI *Unrewarded Windows* (Photostim-Unreinforced, purple) or sessions in which laser illumination was delivered during *Windows of Opportunity* (Photostim-Reinforced, green). Each row represents activity from a single neuron, normalized to baseline (-2 to 0 sec before laser illumination onset), and smoothed with a 50 ms Gaussian. Neurons are sorted according to mean activity during laser illumination (0 to +2 sec). Summary population data in the bottom panels are represented as mean ± SEM. Black marks underneath the population data represent 10 ms steps when the population activity differed between Photostim-Unreinforced vs. Photostim-Reinforced sessions (rank-sum test, $p<0.01$). Axis and color limits are the same as for ChR2 mice in Figure 4 to enable comparison with experimental mice.

(C) Licking activity from all mice contributing recordings for each target area from sessions in which photostimulation was delivered during ITI *Unrewarded Windows* (Photostim-Unreinforced, purple) or sessions in which photostimulation was delivered during *Windows of Opportunity* (Photostim-Reinforced, green). Each row represents activity from a single mouse. Summary population data in the bottom panels are represented as mean ± SEM. Black marks underneath the population data represent 10 ms steps when the population licking activity differed between Photostim-Unreinforced vs. Photostim-Reinforced sessions (rank-sum test, $p<0.01$).

(D) Percents of neurons that were facilitated (solid bars) or suppressed (open bars) in control eYFP mice in each area during Photostim-Unreinforced sessions (purple) or Photostim-Reinforced sessions (green). Denominator n's refer to neurons recorded across all mice during each session type. There were no clear differences in percentages of neurons facilitated or suppressed on Rewarded or Unrewarded days (2-sample tests for equality of proportions: $p>0.10$, corrected for 4 multiple comparisons using Holm's procedure). Axis limits are the same as for ChR2 mice in Figure 4 to enable comparison with experimental mice.

(E) Percents of neurons that were facilitated (solid bars) or suppressed (open bars) in control eYFP mice in each area during Photostim-Unreinforced sessions (left, purple) or Photostim-Reinforced sessions (right, green). Data is replotted from (C) to facilitate comparisons between areas for each session type. There were no clear differences in percentages of neurons facilitated or suppressed between areas (2-sample tests for equality of proportions: $p>0.10$, corrected for 4 multiple comparisons using Holm's procedure). Axis limits are the same as for ChR2 mice in Figure 4 to enable comparison with experimental mice.

Figure S9 Neurons facilitated or suppressed by cholinergic photostimulation may have different baseline firing rates

(A) The baseline firing rates of neurons in ChR2 mice that were either facilitated (solid distributions) or suppressed (open distributions) by photostimulation of cholinergic basal forebrain neurons are plotted by region (dmPFC left, BLA right) and session (Photostim-Unreinforced sessions in purple, Photostim-Reinforced sessions in green). Significant facilitation and suppression were determined based on a sign-rank test comparing activity in the 1 sec before stimulation vs 0-0.5 sec after ($p<0.01$). Given that firing rate distributions were right-skewed, firing rates are displayed as kernel density estimates on a log-scale and were log-transformed prior to analysis. Linear models revealed a main effect of Region ($F_{1,187}=14.56$, ***$p<0.001$; dmPFC neurons had higher baseline firing rates than BLA neurons) and Facilitation vs. Suppression ($F_{1,187}=6.11$, *$p=0.014$; Facilitated neurons had higher baseline firing rates than Suppressed neurons), but no effect of Session or interactions. Exploratory two-sample t-tests revealed that facilitated neurons may have had higher baseline firing rates during the Photostim-Reinforced session in both dmPFC ($t_{33}=2.78$, *$p=0.036$, corrected for 4 multiple comparisons using Holm's procedure) and the BLA ($t_{71}=2.40$, #$p=0.057$, corrected). Data from eYFP mice is not shown given how few neurons passed statistical criteria for significant modulation.

Figure S10 Traces from individual neuron ex vivo slice recordings

Sample traces from individual BLA-mPFC projector neurons (left, magenta) and BLA^{GABA} (right, green) neurons showing membrane potential responses to one second of 5ms pulses of 470 nm light delivered at 5, 10, or 20 Hz in current-clamp. In some cells, photostimulation generated action potentials qualifying them as responsive, however, an EPSP amplitude could not be derived. Of BLA-mPFC projector neurons, 19/19 were qualitatively determined to be responsive. Of BLA^{GABA} neurons, 20/23 were responsive.

Figure 1

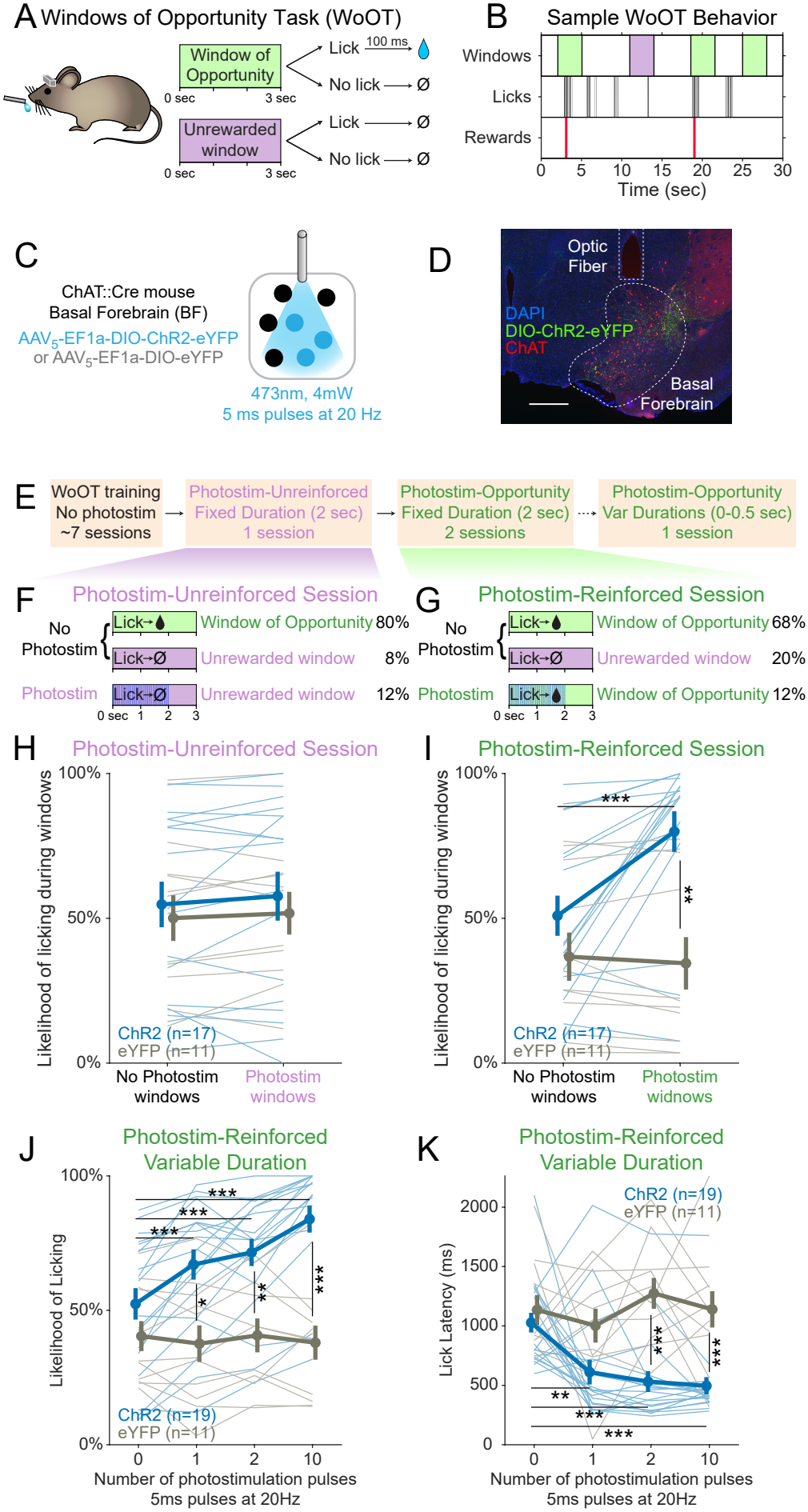
A Windows of Opportunity Task (WoOT)
Window of Opportunity
0 sec
3 sec
Lick
100 ms
No lick
Unrewarded window
Lick
No lick
B Sample WoOT Behavior
Windows
Licks
Rewards
0 5 10 15 20 25 30
Time (sec)
C
ChAT::Cre mouse
Basal Forebrain (BF)
AAV5-EF1a-DIO-ChR2-eYFP
or AAV5-EF1a-DIO-eYFP
473nm, 4mW
5 ms pulses at 20 Hz
D
Optic Fiber
DAPI
DIO-ChR2-eYFP
ChAT
Basal Forebrain
E
WoOT training
No photostim
~7 sessions
Photostim-Unreinforced
Fixed Duration (2 sec)
1 session
Photostim-Opportunity
Fixed Duration (2 sec)
2 sessions
Photostim-Opportunity
Var Durations (0-0.5 sec)
1 session
F Photostim-Unreinforced Session
No Photostim
Lick→
Window of Opportunity 80%
Lick→Ø
Unrewarded window 8%
Photostim
Lick→Ø
Unrewarded window 12%
0 sec 1 2 3
G Photostim-Reinforced Session
No Photostim
Lick→
Window of Opportunity 68%
Lick→Ø
Unrewarded window 20%
Photostim
Lick→
Window of Opportunity 12%
0 sec 1 2 3
H Photostim-Unreinforced Session
Likelihood of licking during windows
100%
50%
0%
ChR2 (n=17)
eYFP (n=11)
No Photostim windows
Photostim windows
I Photostim-Reinforced Session
Likelihood of licking during windows
100%
50%
0%
***
**
ChR2 (n=17)
eYFP (n=11)
No Photostim windows
Photostim widnows
J Photostim-Reinforced Variable Duration
Likelihood of Licking
100%
50%
0%
***
***
***
*
**
***
ChR2 (n=19)
eYFP (n=11)
0 1 2 10
Number of photostimulation pulses
5ms pulses at 20Hz
K Photostim-Reinforced Variable Duration
Lick Latency (ms)
2000
1500
1000
500
0
ChR2 (n=19)
eYFP (n=11)
**
***
***
***
**
***
0 1 2 10
Number of photostimulation pulses
5ms pulses at 20Hz

Figure 2

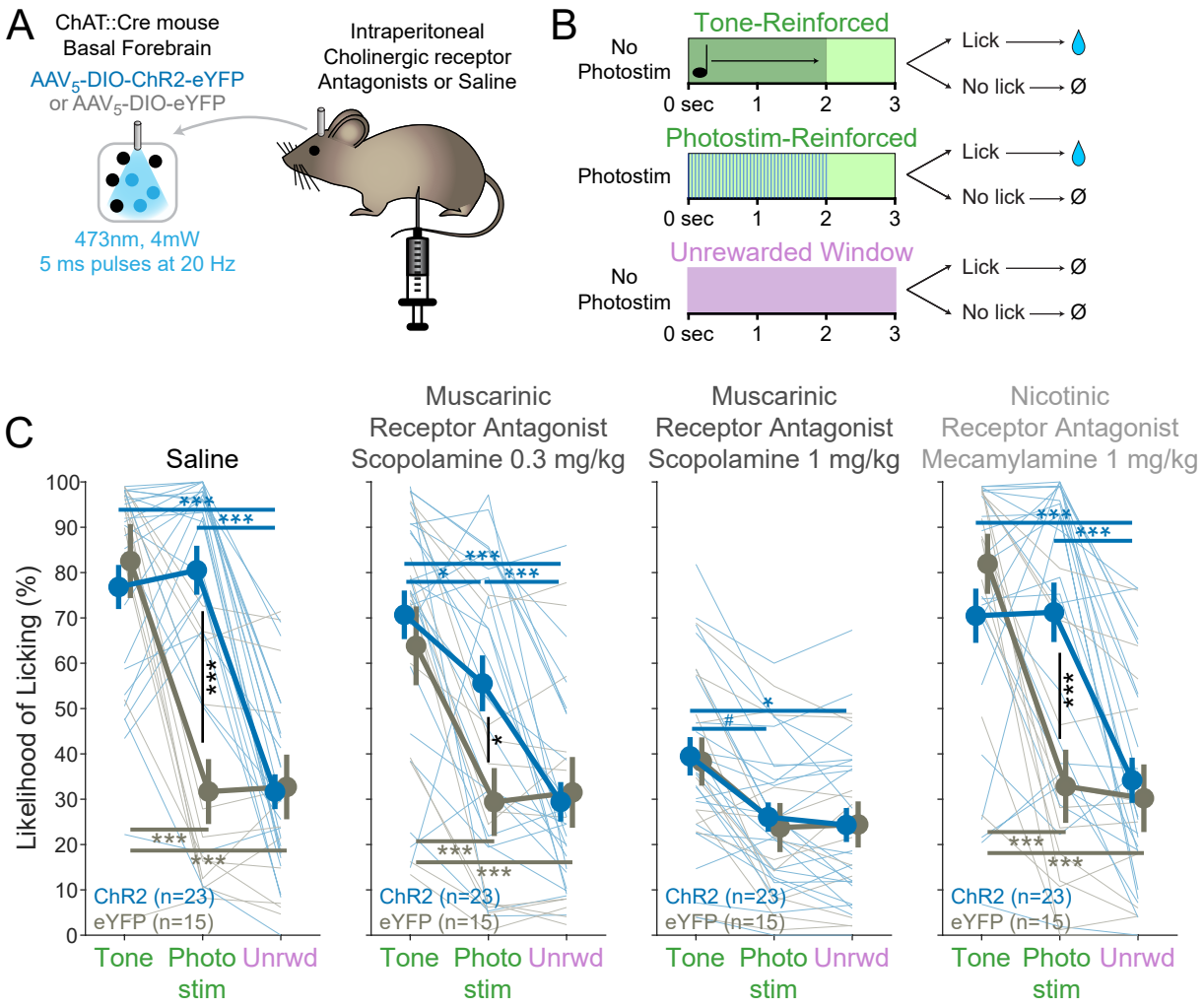
A
ChAT::Cre mouse
Basal Forebrain
AAV5-DIO-ChR2-eYFP
or AAV5-DIO-eYFP
473nm, 4mW
5 ms pulses at 20 Hz
Intraperitoneal
Cholinergic receptor
Antagonists or Saline
B
Tone-Reinforced
No Photostim
0 sec 1 2 3
Lick
No lick
Photostim-Reinforced
Photostim
Unrewarded Window
C
Saline
Muscarinic Receptor Antagonist Scopolamine 0.3 mg/kg
Muscarinic Receptor Antagonist Scopolamine 1 mg/kg
Nicotinic Receptor Antagonist Mecamylamine 1 mg/kg
Likelihood of Licking (%)
ChR2 (n=23)
eYFP (n=15)
Tone
Photo stim
Unrwd

Figure 3

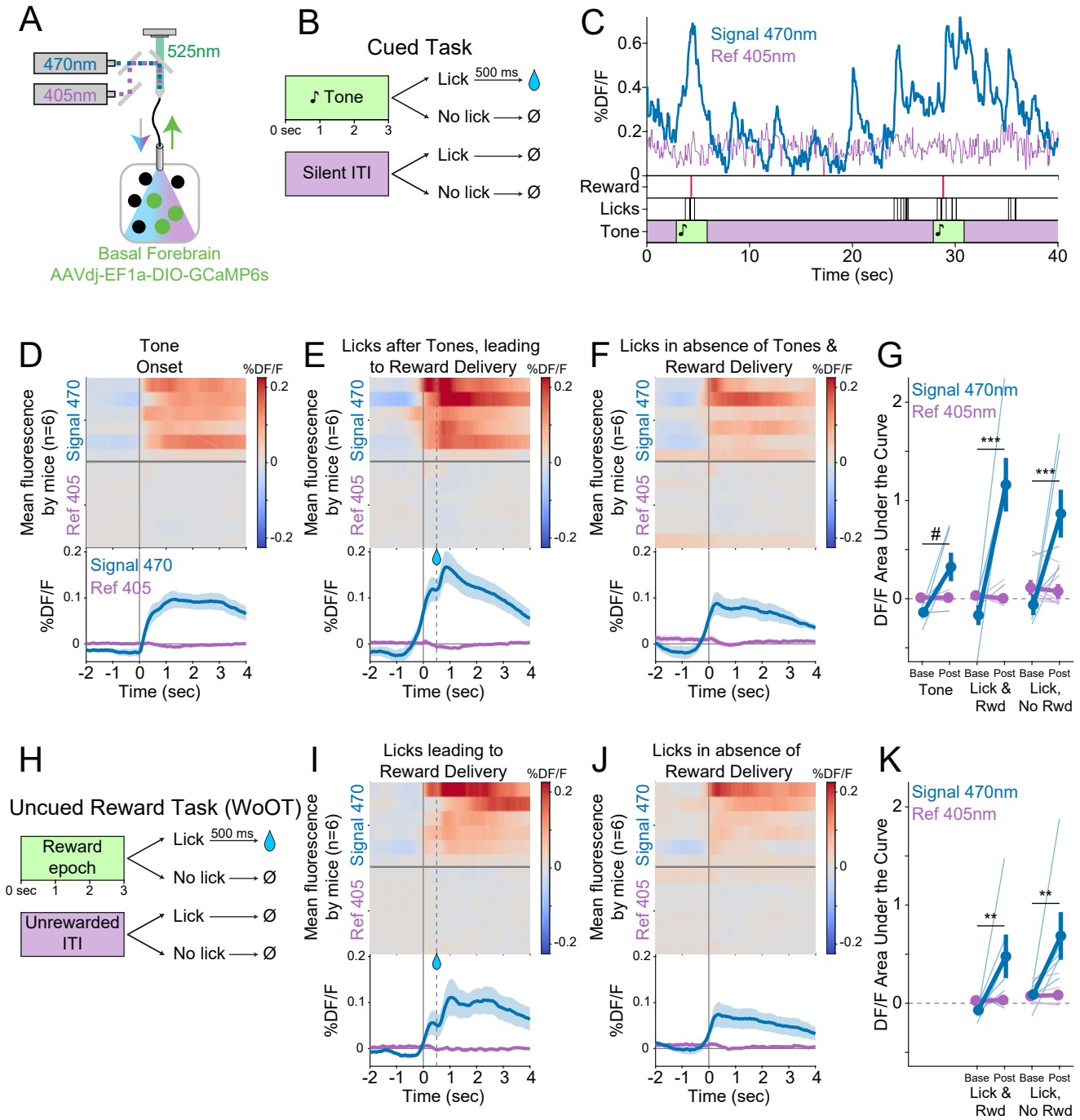
A
470nm
405nm
525nm
Basal Forebrain
AAVdj-EF1a-DIO-GCaMP6s
B
Cued Task
Tone
0 sec 1 2 3
Lick 500 ms
No lick
Silent ITI
Lick
No lick
C
Signal 470nm
Ref 405nm
%DF/F
Reward
Licks
Tone
Time (sec)
D
Tone Onset
Mean fluorescence by mice (n=6)
Signal 470
Ref 405
%DF/F
Signal 470
Ref 405
Time (sec)
E
Licks after Tones, leading to Reward Delivery
F
Licks in absence of Tones & Reward Delivery
G
Signal 470nm
Ref 405nm
DF/F Area Under the Curve
Base Post Base Post Base Post
Tone
Lick & Rwd
Lick, No Rwd
H
Uncued Reward Task (WoOT)
Reward epoch
0 sec 1 2 3
Lick 500 ms
No lick
Unrewarded ITI
Lick
No lick
I
Licks leading to Reward Delivery
J
Licks in absence of Reward Delivery
K
Signal 470nm
Ref 405nm
DF/F Area Under the Curve
Base Post Base Post
Lick & Rwd
Lick, No Rwd

Figure 4

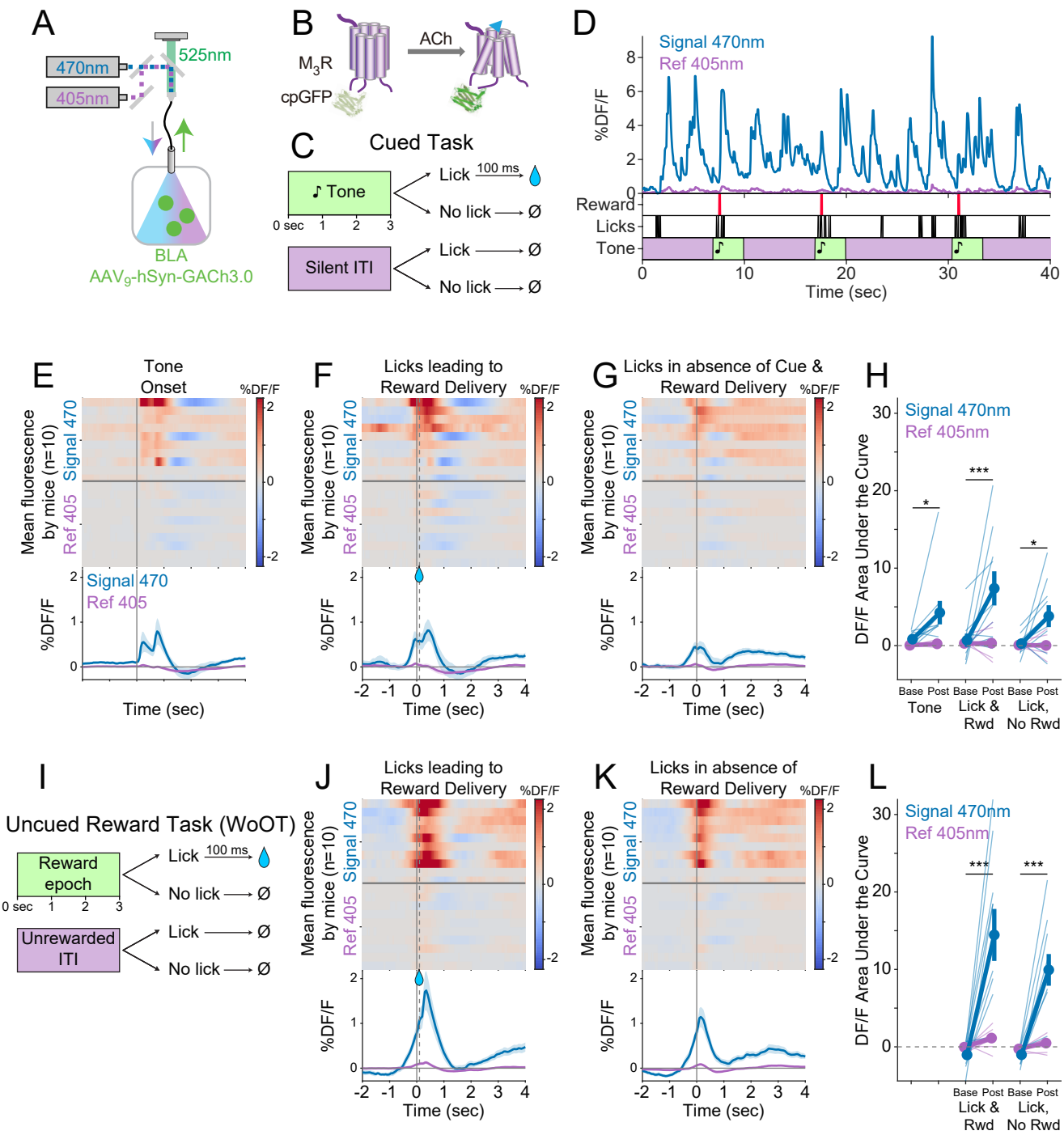
A
470nm
405nm
525nm
BLA
AAV9-hSyn-GACh3.0
B
M3R
cpGFP
ACh
C
Cued Task
Tone
0 sec 1 2 3
Lick
100 ms
No lick
Silent ITI
Lick
No lick
D
Signal 470nm
Ref 405nm
%DF/F
Reward
Licks
Tone
Time (sec)
E
Tone Onset
Mean fluorescence by mice (n=10)
Signal 470
Ref 405
%DF/F
Signal 470
Ref 405
Time (sec)
F
Licks leading to Reward Delivery
G
Licks in absence of Cue & Reward Delivery
H
Signal 470nm
Ref 405nm
DF/F Area Under the Curve
Base Post Base Post Base Post
Tone
Lick & Rwd
Lick, No Rwd
I
Uncued Reward Task (WoOT)
Reward epoch
0 sec 1 2 3
Lick
100 ms
No lick
Unrewarded ITI
Lick
No lick
J
Licks leading to Reward Delivery
K
Licks in absence of Reward Delivery
L
Signal 470nm
Ref 405nm
DF/F Area Under the Curve
Base Post Base Post
Lick & Rwd
Lick, No Rwd

Figure 5

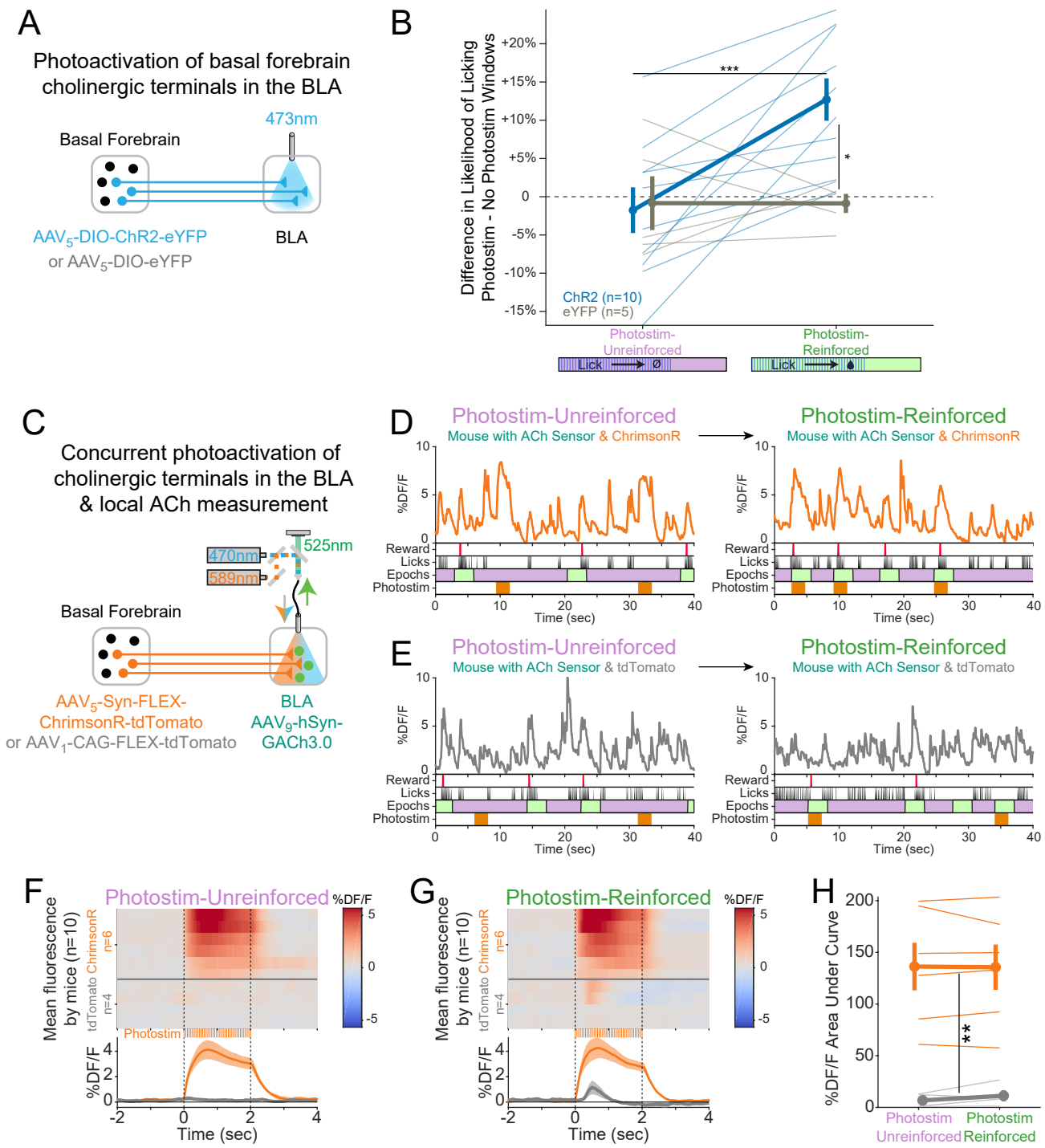
A
Photoactivation of basal forebrain cholinergic terminals in the BLA
473nm
Basal Forebrain
AAV5-DIO-ChR2-eYFP
or AAV5-DIO-eYFP
BLA
B
Difference in Likelihood of Licking
Photostim - No Photostim Windows
+20%
+15%
+10%
+5%
0
-5%
-10%
-15%
***
*
ChR2 (n=10)
eYFP (n=5)
Photostim-Unreinforced
Photostim-Reinforced
Lick
C
Concurrent photoactivation of cholinergic terminals in the BLA & local ACh measurement
470nm
589nm
525nm
Basal Forebrain
AAV5-Syn-FLEX-ChrimsonR-tdTomato
or AAV1-CAG-FLEX-tdTomato
BLA
AAV9-hSyn-GACh3.0
D
Photostim-Unreinforced
Mouse with ACh Sensor & ChrimsonR
Photostim-Reinforced
Mouse with ACh Sensor & ChrimsonR
%DF/F
Reward
Licks
Epochs
Photostim
Time (sec)
E
Photostim-Unreinforced
Mouse with ACh Sensor & tdTomato
Photostim-Reinforced
Mouse with ACh Sensor & tdTomato
F
Photostim-Unreinforced
Mean fluorescence by mice (n=10)
ChrimsonR n=6
tdTomato n=4
Photostim
%DF/F
Time (sec)
G
Photostim-Reinforced
H
%DF/F Area Under Curve
**
Photostim Unreinforced
Photostim Reinforced

Figure 6

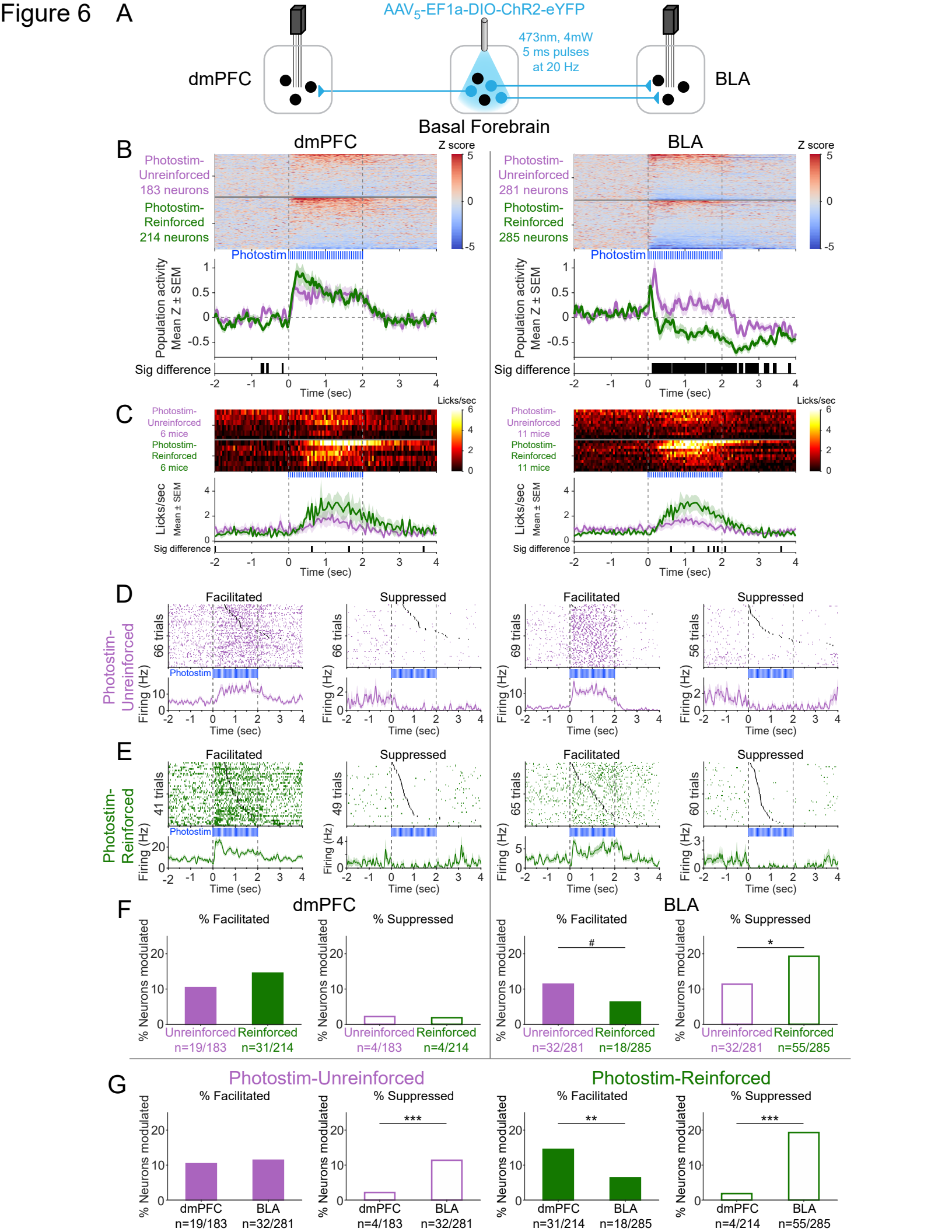
A
AAV5-EF1a-DIO-ChR2-eYFP
473nm, 4mW
5 ms pulses
at 20 Hz
dmPFC
BLA
Basal Forebrain
B
dmPFC
BLA
Z score
Photostim-
Unreinforced
183 neurons
Photostim-
Reinforced
214 neurons
281 neurons
285 neurons
Photostim
Population activity
Mean Z ± SEM
Sig difference
Time (sec)
C
Licks/sec
Photostim-
Unreinforced
6 mice
Photostim-
Reinforced
6 mice
11 mice
Licks/sec
Mean ± SEM
D
Facilitated
Suppressed
Photostim-
Unreinforced
66 trials
69 trials
56 trials
Firing (Hz)
E
Photostim-
Reinforced
41 trials
49 trials
65 trials
60 trials
F
dmPFC
BLA
% Facilitated
% Suppressed
% Neurons modulated
Unreinforced
Reinforced
n=19/183
n=31/214
n=4/183
n=4/214
n=32/281
n=18/285
n=32/281
n=55/285
#
*
G
Photostim-Unreinforced
Photostim-Reinforced
dmPFC
BLA
n=19/183
n=32/281
n=4/183
n=32/281
n=31/214
n=18/285
n=4/214
n=55/285
***
**

Figure 7

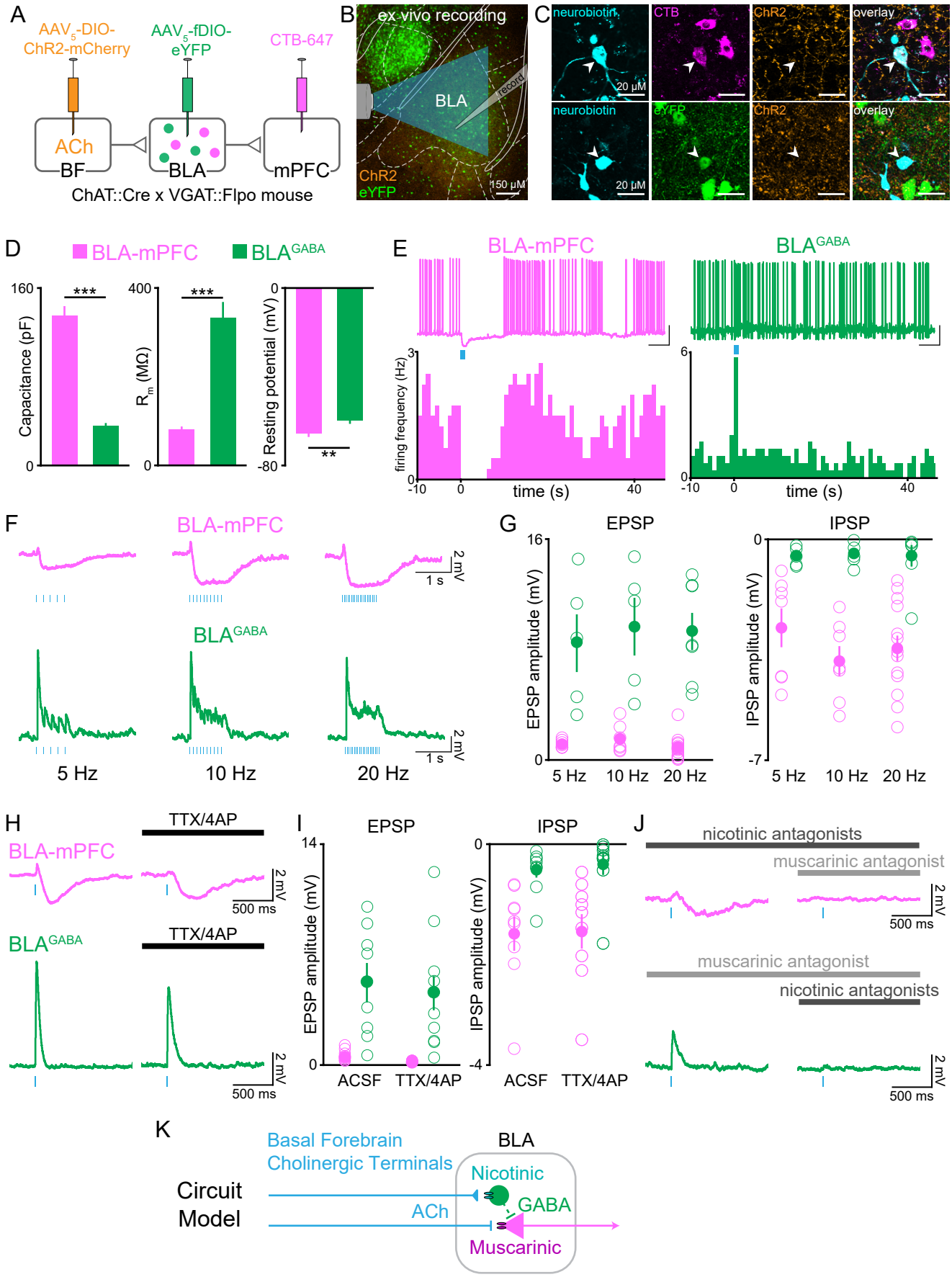
A
AAV5-DIO-ChR2-mCherry
AAV5-fDIO-eYFP
CTB-647
ACh
BF
BLA
mPFC
ChAT::Cre x VGAT::Flpo mouse
B
ex vivo recording
BLA
record
ChR2
eYFP
150 µM
C
neurobiotin
CTB
ChR2
overlay
20 µM
D
BLA-mPFC
BLAGABA
Capacitance (pF)
Rm (MΩ)
Resting potential (mV)
***
**
E
BLA-mPFC
BLAGABA
firing frequency (Hz)
time (s)
F
BLA-mPFC
BLAGABA
2 mV
1 s
5 Hz
10 Hz
20 Hz
G
EPSP
IPSP
EPSP amplitude (mV)
IPSP amplitude (mV)
5 Hz
10 Hz
20 Hz
H
TTX/4AP
BLA-mPFC
BLAGABA
2 mV
500 ms
I
EPSP
IPSP
EPSP amplitude (mV)
IPSP amplitude (mV)
ACSF
TTX/4AP
J
nicotinic antagonists
muscarinic antagonist
2 mV
500 ms
K
Circuit Model
Basal Forebrain Cholinergic Terminals
BLA
Nicotinic
GABA
ACh
Muscarinic